FISEVIER

Contents lists available at ScienceDirect

Acta Biomaterialia

journal homepage: www.elsevier.com/locate/actbio



Full length article

Comparative *in vitro* study on binary Mg-RE (Sc, Y, La, Ce, Pr, Nd, Sm, Eu, Gd, Tb, Dy, Ho, Er, Tm, Yb and Lu) alloy systems



Jianing Liu^{a,1}, Dong Bian^{b,c,1}, Yufeng Zheng^{a,b,*}, Xiao Chu^c, Yulin Lin^d, Ming Wang^e, Zefeng Lin^f, Mei Li^c, Yu Zhang^{c,**}, Shaokang Guan^{g,**}

- ^a Academy for Advanced Interdisciplinary Studies, Peking University, Beijing 100871, China
- b Department of Materials Science and Engineering, College of Engineering, Peking University, No.5 Yi-He-Yuan Road, Hai-Dian District, Beijing 100871, China
- ^c Department of Orthopedics, Guangdong Provincial People's Hospital, Guangdong Academy of Medical Sciences, Guangzhou 510080, China
- ^d Department of Orthopedics, The Fifth Affiliated Hospital of Guangzhou Medical University, Guangdong 510700, China
- ^eThe First School of Clinical Medicine, Southern Medical University, Guangdong 510010, China
- ^f Guangdong Key Lab of Orthopedic Technology and Implant Materials Key Laboratory of Trauma & Tissue Repair of Tropical Area of PLA Department of Orthopedics, Guangzhou School of Clinical Medicine, Southern Medical University (Guangzhou General Hospital of Guangzhou Military Command of PLA), Guangdong 510010, China
- g School of Materials Science and Engineering, Zhengzhou University, Zhengzhou 450001, China

ARTICLE INFO

Article history: Received 17 July 2019 Revised 3 November 2019 Accepted 6 November 2019 Available online 10 November 2019

Key words:
Mg-RE alloy
Alloy design
Mechanical property
Corrosion behavior
Biocompatibility

ABSTRACT

Correct selection of alloying elements is important for developing novel biodegradable magnesium alloys with superior mechanical and biological performances. In contrast to various reports on nutrient elements (Ca, Zn, Sr, etc.) as alloying elements of biomedical magnesium alloys, there is limited information about how to choose the right rare earth elements (REEs) as alloying elements of magnesium. In this work, 16 kinds of REEs were individually added into Mg, including Sc, Y, La, Ce, Pr, Nd, Sm, Eu, Gd, Tb, Du, Ho, Er, Tm, Yb and Lu, to fabricate binary Mg-RE model alloys with different composition points. Under the same working history, comparative studies were undertaken and the impact of each kind of rare earth element on the microstructure, mechanical property, corrosion behavior and biocompatibility of Mg were investigated. The corresponding influence level for the 16 kinds of REEs were ranked. The results showed that the second phases were detected in some Mg-RE alloys, which were mainly composed of Mg₁₂RE. By adding different REEs into Mg with proper contents, the mechanical properties of resulting Mg-RE binary alloys could be adjusted in wide range. The corrosion resistance of Mg-light REE alloys was generally better than Mg-heavy REE alloys. As for biocompatibility, Mg-RE model alloys showed no cytotoxic effect on MC3T3-E1 cells. The hemolysis rates of all experimental Mg-RE model alloys were lower than 5% except for Mg-Lu alloy model. In general, the addition of different REEs into Mg could improve its performance from different aspects. This work provides a better understanding on suitable REEs as alloying elements for magnesium, and the future R&D direction on biomedical Mg-RE alloys was proposed.

Statement of Significance

In contrast to various reports on nutrient elements (Ca, Zn, Sr, etc.) as alloying elements of biomedical magnesium alloys, until now there is limited information about how to choose the right rare earth elements (REEs) as alloying elements of magnesium. In this work, comparative studies were undertaken by individually adding 16 kinds of REEs, including Sc, Y, La, Ce, Pr, Nd, Sm, Eu, Gd, Tb, Du, Ho, Er, Tm, Yb and Lu, into Mg to fabricate binary Mg-RE model alloys, with different composition points, then the impact

^{*} Corresponding author at: Department of Materials Science and Engineering, College of Engineering, Peking University, No.5 Yi-He-Yuan Road, Hai-Dian District, Beijing 100871, China.

^{**} Corresponding authors.

E-mail addresses: yfzheng@pku.edu.cn (Y. Zheng), skguan@zzu.edu.cn (S. Guan).

 $^{^{\}mbox{\scriptsize 1}}$ These two authors contributed equally to this study.

of each kind of rare earth element on the microstructure, mechanical property, corrosion behavior and biocompatibility of Mg under the same working history were investigated, and the corresponding influence level for the 16 kinds of REEs were ranked. This work provides a better understanding on suitable REEs as alloying elements for magnesium, and the future R&D direction on biomedical Mg-RE alloys was proposed.

© 2019 Acta Materialia Inc. Published by Elsevier Ltd. All rights reserved.

1. Introduction

The research and development of magnesium and its alloys as degradable bioimplants has become the hot topic in the field of metallic biomaterial science and engineering in the 21st century. As one of the essential macro elements in the human body, magnesium is desirable for its superior biocompatibility, favorable biodegradability and superior osteogenesis [1,2]. However, the rapid degradation rate caused by the presence of impurities (Fe, Ni, Cu) in Mg and the insufficient mechanical strength impede its development [3,4]. Alloying is a convenient and commonused method to make up these deficiencies [5]. Until now, many biomedical magnesium alloy systems have been investigated, mainly focused on the nutrient elements such as Ca, Zn, Sr, Si, etc. [6–8]. However, these newly-developed magnesium alloys have shown mechanical properties at the level as ultimate tensile strength lower than 280 MPa and elongation less than 20% on the whole [9]. Besides, due to the low solid solubilities of some alloying elements (e.g. Si) in Mg, the addition of these elements could lead to the precipitation of the second phase, introduced galvanic corrosion and might accelerate the degradation of corresponding Mg alloys in the body fluids.

To further enhance the strength, rare earth elements (REEs) were considered to be added into Mg. The REE group is comprised of seventeen rare earth elements in the periodic table, specifically fifteen lanthanides (Ce, Dy, Er, Eu, Gd, Ho, La, Lu, Nd, Pr, Pm, Sm, Tb, Tm and Yb) as well as Sc and Y, whose properties are similar to lanthanides. Generally, the REEs are divided into two groups: (i) light REE (La, Ce, Pr, Nd and Pm) and (ii) heavy REE (Sm, Eu, Gd, Tb, Dy, Ho, Er, Tm, Yb and Lu) [5]. As alloying elements of Mg, the REEs could be classified into (i) high solid solubilities (Y, Gd, Tb, Dy, Ho, Er, Tm, Yb and Lu) and (ii) limited solid solubilities (Nd, La, Ce, Pr, Sm and Eu) [5]. It should be noted that Eu is the only REE which has no solid solubility in Mg. The maximum solid solubilities of REEs in Mg are displayed in Fig. 1. According to the phase diagrams of binary magnesium alloys, the Mg-RE systems were divided into eutectic systems and peritectic system (Mg-Sc system). The eutectic systems could be subdivided according to the solid solubilities of REEs in Mg.

In fact, it has been reported that the addition of REEs could effectively improve the mechanical properties and corrosion resistance of resulting magnesium alloys [10,11]. From the viewpoint of metallurgy, during the melting process, the REEs could combine with the impurities (Fe, Ni, Cu, etc.) in magnesium rapidly, and deposit to the bottom of melt. Thus, the presence of REEs is conducive to hydrogen, oxygen, sulfur and impurities removal in magnesium melt, which could finally purify the melt. This effect is socalled "the scavenger effect". Since the presence of small amounts of sensitive impurities could damage the corrosion resistance of magnesium alloys once the impurities contents exceed the tolerance limits [12], it is believed that the scavenger effect of REEs could effectively improve the corrosion resistance of magnesium alloys. In addition, the REEs could incorporate into the corrosion layer, improve the stability and integrity of the surface film, and finally enhance the corrosion resistance of magnesium alloys [13].

Until now, the reports on binary Mg-RE alloys being investigated were scattered, including Mg-Sc, Mg-Y, Mg-La, Mg-Ce, Mg-Nd, Mg-Gd and Mg-Dy alloys [6,14–17]. However, due to the difference in alloys preparation and processing methods, experimental conditions and evaluation methods, as well as the compositions of Mg-RE alloys, data obtained from different studies could not be directly compared with each other. According to the existing reports, it is hard to estimate that how one specific rare earth element, as an alloying element of Mg, contributes to the microstructure, mechanical property, degradation behavior and biological response of alloy. (In this paper, the word "degradation" has the same meaning with the word "corrosion".) In this study, based on the Mg-RE phase diagrams, proper contents of REEs (Sc, Y, La, Ce, Pr, Nd, Sm, Eu, Gd, Tb, Dy, Ho, Er, Tm, Yb and Lu) were added into magnesium respectively, to obtain binary Mg-RE model alloys with the same preparation and processing methods. Under the same experimental conditions, a comparative study on the microstructure, degradation behavior, mechanical property and biocompatibility was carried out to explore the design principles of Mg-RE alloys. It would provide scientific guidance for alloy design of novel biodegradable multiple-component Mg-RE alloy system in the future.

2. Materials and methods

2.1. Material preparation

The composition selection of the experimental binary Mg-RE alloys mainly depends on the maximum solubilities of REEs in Mg, which is displayed in Fig. 1. With respect to the REEs with limited solubilities, low contents of REEs were added into Mg and vice versa. Specifically, as for the REEs whose maximum solubilities are lower than 20 wt.%, that is, La, Pr, Ce, Nd, Sm, Yb and Y, 1 wt.% and 3 wt.% of REEs were added into Mg. It should be noted that the reported maximum solid solubilities of Pr are discrepant [18]. Therefore, an extra Mg-0.5Pr alloy were also studied. As for the REEs whose maximum solubilities are between 20 and 25 wt.%, 1 wt.% and 5 wt.% of REEs were added into Mg, that is, Mg-(1, 5)Gd and Mg-(1, 5)Tb alloys. As for the REEs whose maximum solubilities are above 25 wt.% (Dy, Ho, Er, Tm, Lu), 1 wt.% and 10 wt.% of REEs were added. The above binary Mg-RE (RE=Sc, Y, La, Ce, Pr, Nd, Sm, Eu, Gd, Tb, Dy, Ho, Er, Tm, Yb and Lu) alloys were melted with bulk pure Mg (99.9 wt.%) and pure rare earths (99.5 wt.%, industrial grade) in medium-frequency induction melting furnace under argon (Ar) atmosphere. All the raw metals were supplied by Hunan Rare-earth Material Research Institute. It should be noted that as a radioactive element created artificially, Pm was not considered in this study. The graphite crucible was heated to the temperature higher than the melting point of alloy by about 50-100 °C, holding for 20 min with stirring. The liquid metal was poured into a graphite mold which had already been preheated to 250 °C and generally cooled with furnace to room temperature. Pure Mg was melted in the same way as a control group. The impurity contents in binary Mg-RE alloys and pure Mg were measured by inductively coupled plasma-atomic emission spectrometry (ICP-AES). The contents of the alloying elements were determined by titration

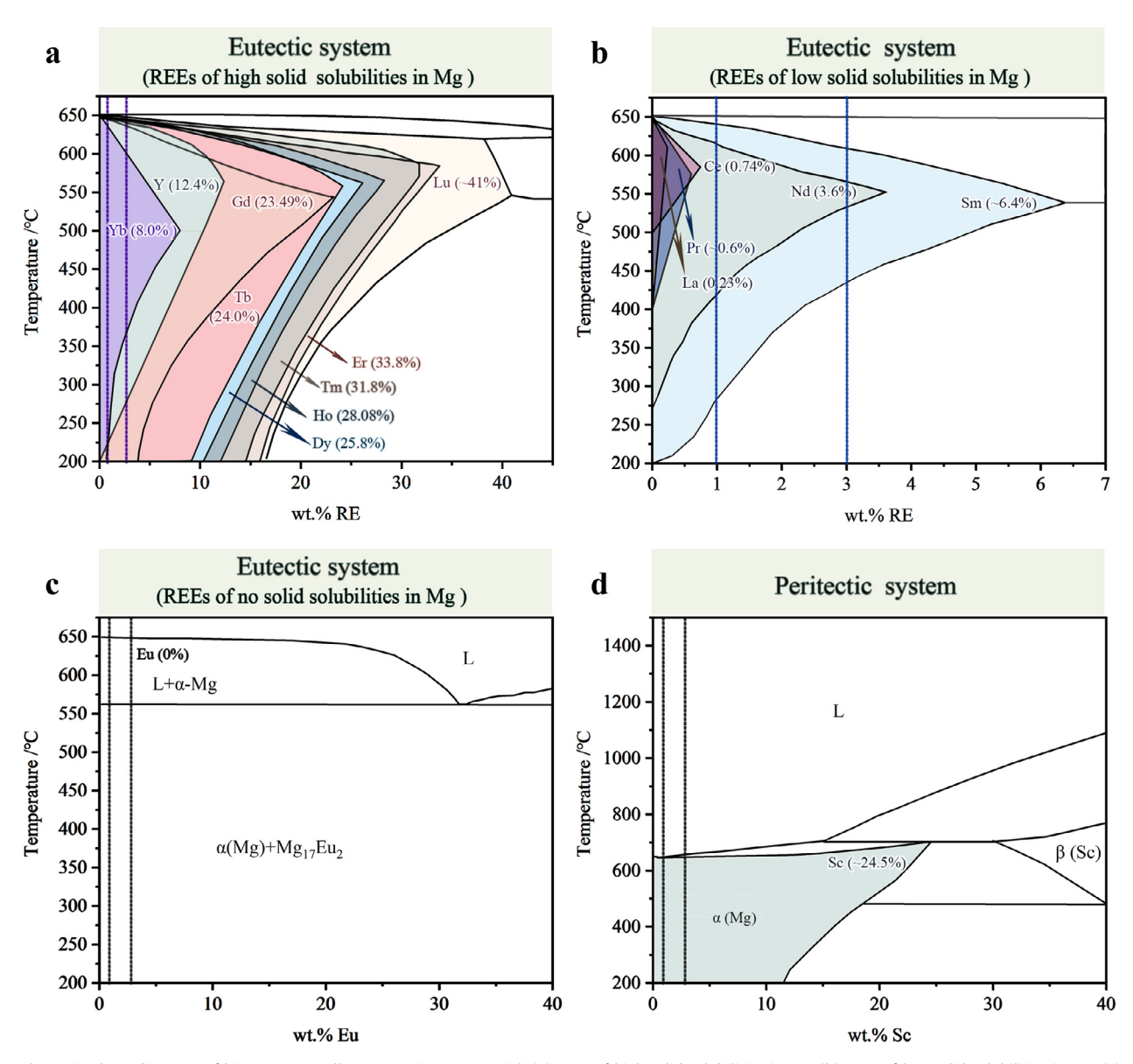


Fig. 1. Schematic phase diagrams of binary Mg-RE alloys. Eutectic systems with (a) REEs of high solid solubilities in Mg. (b) REEs of low solid solubilities in Mg. (c) REEs of no solid solubilities in Mg. (d) peritectic system. Two vertical lines in each graph corresponds to the composition points of 1 wt.% and 3 wt.%, respectively.

method. The nominal and actual compositions of them are shown in Table 1.

The billets were machined into cylinders with a dimension of Φ $39.6 \times 50 \, \text{mm}$ and then solid-solution treatment was conducted for 4h with water cooling. The solid-solution process was carried out in muffle furnace in air. The heat temperature was dependent on the rare earth contents of alloys. As for magnesium alloys with low addition of RE (including Mg-1Sc, Mg-1Y, Mg-1La, Mg-1Ce, Mg-0.5Pr, Mg-1Pr, Mg-1Nd, Mg-1Sm, Mg-1Eu, Mg-1Gd, Mg-1Tb, Mg-1Dy, Mg-1Ho, Mg-1Er, Mg-1Tm, Mg-1Yb and Mg-1Lu), the heattreatment was conducted at 450 °C. The other alloys were heattreated at 500 °C. After preheating at 400 °C for 20 min, the alloys were extruded with an extrusion rate of 2 mm/s. The principle of extrusion temperature selection is mainly in accordance with the phase diagram of binary Mg-RE alloys. The extrusion temperature should be lower than the melting point of the eutectic alloy. And in order to avoid phase transformation during extrusion process, it would be better if the phase transformation temperature of alloy is in single-phase region and is higher than the phase transformation temperature to some extent. Besides, since the ductility of magnesium alloys is comparatively high in certain temperature range, the extrusion temperature should be within this range to avoid cracks caused by the inferior ductility. Last but not least, the deformation resistance is also an important factor which is primarily influenced by the extrusion temperature and needs to be considered. Otherwise, if the deformation resistance of alloys exceeds the capacity of extruder, the extrusion process could not be carried out normally. Since the phase diagrams, temperature range for high ductility as well as the deformation resistance of our 34 kinds of binary Mg-RE alloys are somewhat different, it would be tough to keep the extrusion temperature constant. The extrusion temperature of the experimental alloys was 350 °C except several alloys, that is, Mg-1Ce, Mg-1Er, Mg-1Dy and Mg-1Nd alloys, whose extrusion temperature was 320 °C. After single-pass extrusion, the alloy rods with a diameter of 12 mm were obtained. As for the control group, the homogenization and extrusion temperatures of pure Mg were 400 °C and 350 °C, respectively. The rods were cut into disks with a thickness of 1.5 mm for microstructural characterization, corrosion

Table 1Nominal and actual compositions of binary Mg-RE alloys and pure Mg as well as their phase constituents.

Material	Composition (wt.%)						Constituent phases	
	RE	Fe	Cu	Ni	Si	Mg		
Pure Mg	1	0.0048	0.0020	0.0001	0.011	Bal.	α-Mg	
Mg-1Sc	0.88	0.015	0.0041	0.0033	0.0089	Bal.	α-Mg	
Mg-3Sc	2.81	0.014	0.0038	0.0032	0.0095	Bal.	α-Mg	
Mg-1Y	1.21	0.013	0.0027	0.0025	0.0087	Bal.	α-Mg	
Mg-3Y	2.90	0.011	0.0032	0.0023	0.0082	Bal.	α-Mg	
Mg-1La	0.98	0.021	0.0052	0.0022	0.0059	Bal.	α -Mg+Mg ₁₂ La	
Mg-3La	3.35	0.019	0.0047	0.0020	0.0053	Bal.	α -Mg+Mg ₁₂ La	
Mg-1Ce	1.09	0.011	0.0057	0.0021	0.0049	Bal.	α -Mg+Mg ₁₂ Ce	
Mg-3Ce	2.86	0.012	0.0051	0.0023	0.0048	Bal.	α -Mg+Mg ₁₂ Ce	
Mg-0.5Pr	0.53	0.027	0.0041	0.0017	0.0051	Bal.	α -Mg+Mg ₁₂ Pr	
Mg-1Pr	1.06	0.0030	0.0045	0.0014	0.0059	Bal.	α -Mg+Mg ₁₂ Pr	
Mg-3Pr	2.79	0.022	0.0051	0.0019	0.0047	Bal.	α -Mg+Mg ₁₂ Pr	
Mg-1Nd	1.19	0.015	0.0052	0.0017	0.0050	Bal.	α -Mg+Mg ₁₂ Nd	
Mg-3Nd	3.11	0.018	0.0057	0.0021	0.0051	Bal.	α -Mg+Mg ₁₂ Nd	
Mg-1Sm	1.17	0.0085	0.0072	0.0029	0.0029	Bal.	α -Mg+Mg ₄₁ Sm ₅	
Mg-3Sm	3.17	0.0081	0.0056	0.0032	0.0033	Bal.	α -Mg+ Mg ₄₁ Sm ₅	
Mg-1Eu	1.29	0.0018	0.0039	0.0025	0.0047	Bal.	α -Mg+Mg ₁₇ Eu ₂	
Mg-3Eu	2.94	0.0021	0.0045	0.0026	0.0052	Bal.	α -Mg+Mg ₁₇ Eu ₂	
Mg-1Gd	1.05	0.0091	0.0041	0.0018	0.0038	Bal.	α-Mg	
Mg-5Gd	4.88	0.0079	0.0035	0.0022	0.0037	Bal.	α-Mg	
Mg-1Tb	1.19	0.0035	0.0018	0.0015	0.0027	Bal.	α-Mg	
Mg-5Tb	4.73	0.0038	0.0019	0.0017	0.0031	Bal.	α-Mg	
Mg-1Dy	1.19	0.0025	0.0017	0.0010	0.0024	Bal.	α-Mg	
Mg-10Dy	9.17	0.0020	0.0014	0.0011	0.0022	Bal.	α-Mg	
Mg-1Ho	1.15	0.0075	0.0025	0.0017	0.0042	Bal.	α-Mg	
Mg-10Ho	9.05	0.0076	0.0021	0.0018	0.0045	Bal.	α-Mg	
Mg-1Er	1.07	0.0054	0.0019	0.0020	0.0039	Bal.	α-Mg	
Mg-10Er	8.78	0.0057	0.0022	0.0021	0.0042	Bal.	α-Mg	
Mg-1Tm	1.02	0.0017	0.0066	0.0029	0.0055	Bal.	α-Mg	
Mg-10Tm	9.12	0.0014	0.0068	0.0028	0.0051	Bal.	α -Mg+Mg ₂₄ Tm ₅	
Mg-1Yb	0.96	0.0025	0.0071	0.0032	0.0057	Bal.	α-Mg	
Mg-3Yb	2.77	0.0029	0.0065	0.0031	0.0055	Bal.	α -Mg+Mg ₂ Yb	
Mg-1Lu	1.17	0.0039	0.0042	0.0018	0.0032	Bal.	α-Mg	
Mg-10Lu	9.55	0.0045	0.0040	0.0017	0.0039	Bal.	α-Mg+Mg ₂₄ Lu ₅	

measurement and cytotoxicity testing. All specimens were polished to 2000 grit by SiC abrasive paper, cleaned in ethanol and dried in air.

2.2. Microstructural characterization

Samples for microstructural characterization were polished by 0.5 µm diamond polishing paste. After ultrasonic cleaning in absolute ethanol, 4% nitric acid alcohol solution or nitric acid solution was adopted for etching. The microstructures were observed under an optical microscope (BX51M, Olympus). For further study, the microstructures of Mg-(0.5, 1)Pr alloys were also observed under SEM (S-4800 cold-cathode field-emission scanning electron microscope, Hitachi).

To analyze the phase constituents of binary Mg-RE alloys, X-ray diffractometer was conducted with Cu K α radiation. The tube voltage and current were 40 kV and 100 mA, respectively. The scanning range is $10^{\circ}-90^{\circ}$ and the scanning rate was $2^{\circ}/$ min. The results were analyzed in Jade software to confirm the phase constituents. The average grain sizes of alloys were calculated according to ASTM E112-13 [19]. Linear intercept method was adopted and image J software (version 1.51 j8, USA) was used. At least three measurements were carried out for each alloy.

2.3. Mechanical property

Specimens for tensile test were machined along the extrusion direction and the dimensions were in accordance with ASTM E8-04 [20]. Longitudinal tensile tests were conducted using the specimens with a gage length of 25 mm, a gauge width of 6 mm, and a gauge thickness of 2 mm. The universal testing machine

(Instron 5969, USA) was adopted at a crosshead speed of 1 mm/min at room temperature. The ultimate tensile strength (UTS), yield strength (YS) and elongation at fracture of alloys were obtained from the stress-strain curves. At least three samples were tested for each alloy. The fractured specimens were observed by SEM to analyze the fracture modes and fracture characteristics of experimental Mg-RE model alloys.

2.4. In vitro degradation test

2.4.1. Electrochemical evaluation

A traditional three-electrode cell system was adopted. The specimens, saturated calomel electrode (SCE) and platinum electrode acted as the working electrode, reference electrode as well as the counter electrode, respectively. The electrochemical workstation (Metrohm Ltd, Switzerland) was applied and Hank's solution (NaCl 8.0 g/L, CaCl₂ 0.14 g/L, KCl 0.4 g/L, NaHCO₃ 0.35 g/L, Glucose 1.0 g/L, MgCl₂•6H₂O 0.1 g/L, Na₂HPO₄•2H₂O 0.06 g/L, KH₂PO₄ 0.06 g/L, MgSO₄•7H₂O 0.06 g/L) was adopted as electrolyte. At room temperature, the open circuit potential was constantly monitored for 3600 s. Afterwards, the potentiodynamic polarization (PDP) was conducted from –500 mV (vs. SCE) to 1000 mV (vs. SCE) at a scanning rate of 0.001 V/s. The corrosion current density was calculated according to ASTM G102-89 [21]. Three duplicates of each group were adopted for electrochemical test.

2.4.2. Immersion test

The immersion test was carried out in accordance with ASTM G31-71 [22]. Prior to the immersion test, the weight of each sample was recorded. Hank's solution was selected as the corrosive medium with an exposure ratio of 20 mL/cm² for 360 h at

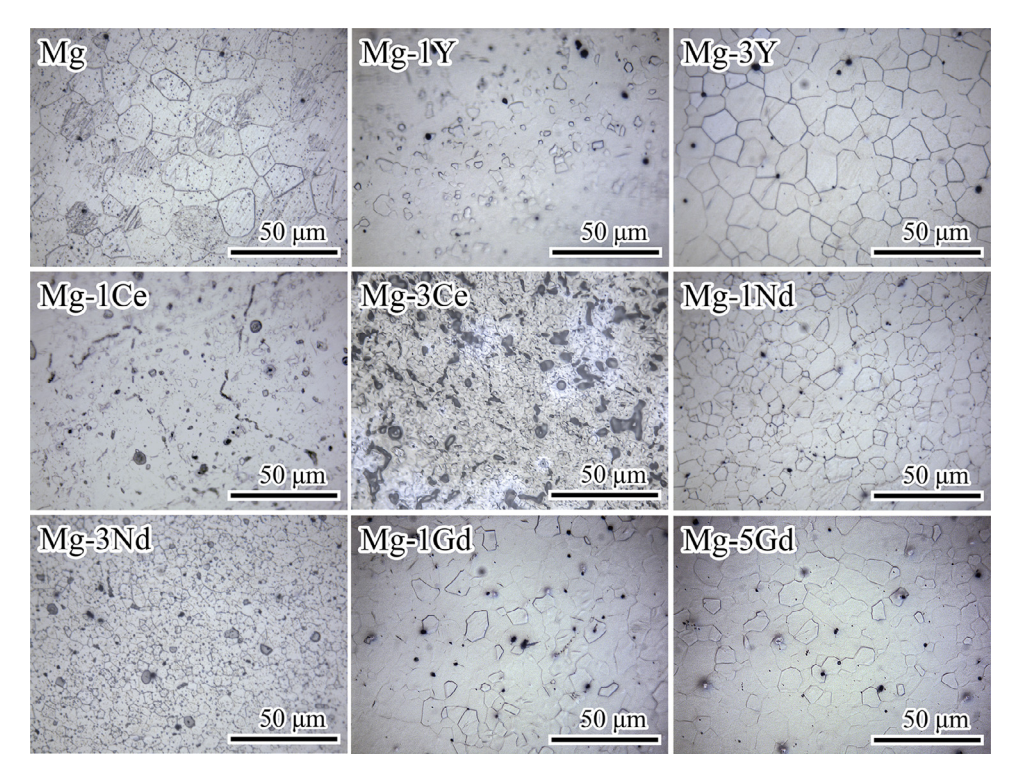


Fig. 2. Optical microstructures of typical Mg-RE model alloys and pure Mg.

37 °C. The pH values were measured periodically by a pH meter (Sartorius, Germany). After immersion for 72 and 360 h, the specimens were removed from Hank's solution, rinsed with deionized water and dried in a desiccator. The surface morphologies of alloys after immersion for 72 h and 360 h were observed under SEM. Cross-sectional morphologies of alloys after 72 h immersion were captured by SEM coupled with EDS (Energy dispersive spectrometer) in the second electron (SE) mode. According to ASTM G1-90 [23], to remove the corrosion product of alloys, CrO₃ was used to prepare chromic acid at the concentration of 200 g/L. After immersion for 72 h and 360 h, the corroded alloys were ultrasonic cleaning in chromic acid to remove the corrosion product. The macroscopic morphologies of alloys after removing the corrosion product were captured. In particular, the cross-sectional morphologies of the alloys which showed pitting corrosion after immersion in Hank's solution for 72 h were observed under SEM. Afterwards, the weight of each corroded sample was recorded and the corrosion rates of alloys were calculated according to the following equation [24]:

$$CR = 3.65 \Delta W/\rho$$

 ΔW is the weight loss rate of metal with the unit of mg/cm²/d and ρ is the metal density with the unit of g/cm³. At least three duplicates were measured for statistical analysis.

2.5. Cytotoxicity

Indirect contact cell assay was carried out to evaluate cell viability with MC3T3-E1 cells. 10% fetal bovine serum (FBS), 1% penicillin-streptomycin were added to Dulbecco's modified eagle's medium (DMEM), which was adopted as cell culture medium. Alloys were sterilized by ultraviolet irradiation and then extracted in DMEM with an extraction ratio of 1.25 cm²/mL at 37 °C in cell incubator with 5% CO₂ for 72 h. After centrifugation, the deposit was removed and the supernatant was retained and stored at 4 °C. Cells were cultured in 96 well plate with a density of 5×10^3 per 100 μL for 24 h in cell incubator. Subsequently, the culture medium was

replaced by sample extracts with 1% penicillin-streptomycin. The cell culture medium and culture medium with 10% dimethylsulfoxide (DMSO) were set as the negative and positive control group, respectively. After culturing for 1 and 3 days, sample extracts were substituted by a mixture of cell counting kit-8 (CCK-8, Donjindo, Kumamoto, Japan) and DMEM at a volume ratio of 1:10 and incubated for 1 h. The microplate reader (BIO-RAD 680) was adopted to measure the spectrophotometric absorbance of each well. 3 duplicates of each group were measured for cell viability test.

2.6. Hemolysis and platelet adhesion

In order to evaluate the hemocompatibility of binary Mg-RE model alloys, hemolysis and platelet adhesion test were carried out. Fresh blood from healthy New Zealand rabbits was collected with the addition of 3.8 wt.% sodium citrate at a volume ratio of 9:1. As for hemolysis test, the fresh blood was diluted by PBS at a volume ratio of 4:5. The experimental binary Mg-RE alloys and pure Mg control were separately immersed in 14 mL PBS at centrifuge tubes and water bathed at 37 °C for 30 min. Three duplicates were carried out. Subsequently, 0.2 mL diluted blood was added into each centrifuge tube. For the positive and negative control group, 14 mL deionized water and PBS, both with 0.2 mL diluted blood were adopted, respectively. After 60 min incubation at 37 °C, the experimental alloys were removed and tubes were centrifuged at 3000 rpm for 5 min. The supernatant was transferred to 96-well plates and the absorbance (OD) was measured by the microplate reader (BIO-RAD 680) at a wavelength of 545 nm. The hemolysis rate was calculated by the following formula:

Hemolysis rate

$$= \frac{\text{OD (test group)-OD (negative control)}}{\text{OD (positive control)-OD (negative control)}} \times 100\%$$

As for platelet adhesion test, the fresh blood was centrifuged at 1000 rpm for 15 min to obtain the platelet-rich plasma (PRP) from the upper fluid. The experimental Mg-RE alloys and pure Mg control were placed into the 24-well plates and 0.4 mL PRP was added

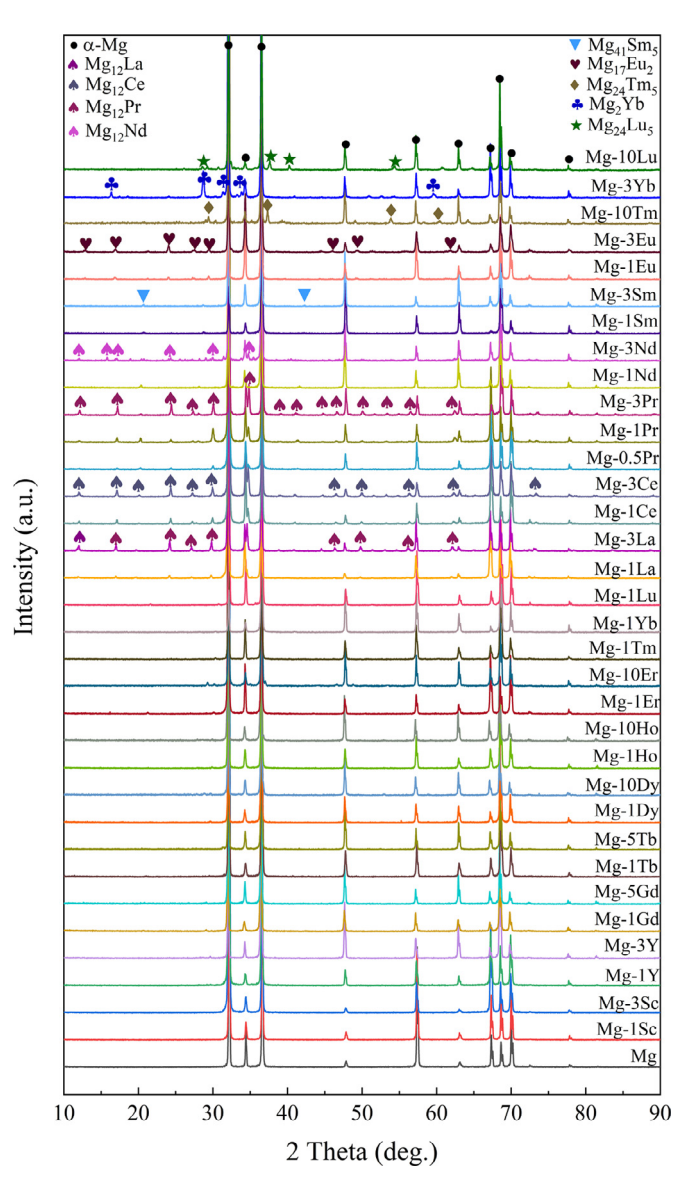


Fig. 3. XRD patterns of binary Mg-RE model alloys and pure Mg.

into each well so that the samples were ensured to be submerged by PRP. After incubation at 37 °C for 60 min, the PRP was removed and the samples were gently rinsed by PBS for three times. The platelets on samples were fixed with 2.5% glutaraldehyde solution for 60 min and dehydrated with gradient alcohol solutions (50%, 60%, 70%, 80%, 90%, 100%) for 10 min each, and finally dried in a desiccator. The morphologies of platelets on samples were observed under SEM.

2.7. Statistical analysis

The experimental results were expressed as mean \pm standard deviations. One-way analysis of variance (ANOVA) followed by Tukey test was carried out for variance analysis. A p-value <0.05 was considered as statistically significant.

3. Results

3.1. Microstructure

Fig. 2 shows the microstructures of typical as-extruded Mg-RE model alloys as well as pure Mg control group. The overall

microstructures of binary Mg-RE model alloys are shown in Fig. S1. Similar to pure Mg, most Mg-RE alloys were fully recrystallized after hot extrusion process and exhibited equiaxed grains without distortion. Among them, the grain sizes of as-extruded Mg-RE model alloys differed with the content of alloying REEs. As for Mg-Y alloys, when yttrium content raised from 1 wt.% to 3 wt.%, the grain size increased from $3.4 \pm 0.4 \,\mu m$ to $10 \pm 3 \,\mu m$. The Mg-Dy alloys showed a similar trend, whose grain sizes increased from $7 \pm 2 \,\mu m$ to $11.3 \pm 0.9 \,\mu m$ with Dy content raised from 1 wt.% to 10 wt.%. While the grain size of some other alloys decreased with higher RE addition, including Mg-Nd (from $8 \pm 1 \,\mu m$ to $4.3 \pm 0.7 \,\mu\text{m}$), Mg-Sm (from $17.6 \pm 0.9 \,\mu\text{m}$ to $10 \pm 1 \,\mu\text{m}$), Mg-Ho (from $10.3 \pm 0.5 \,\mu m$ to $8.3 \pm 0.4 \,\mu m$), Mg-Yb (from $16 \pm 3 \,\mu m$ to $12\pm 2\,\mu m)$ and Mg-Lu (from $14.6\pm 0.8\,\mu m$ to $10\pm 2\,\mu m$). Besides, the addition of elements Gd and Tb did not make too much difference in grain sizes of resulting Mg-RE alloys. Among the recrystallized alloys, the grain sizes of Mg-(1, 3)Nd alloys were much smaller than that of pure Mg ($13\pm2\mu m$). That is, the addition of proper content of Nd into magnesium could effectively refine the grain size. The addition of element Pr and Er also had a similar effect. The grain sizes of Mg-1Er and Mg-10Er alloys were respectively $7.3 \pm 0.8 \,\mu m$ and $7 \pm 1 \,\mu m$. As for Mg-(0.5, 1)Pr alloys, the grain sizes were too small to be discerned under the optical microscope so that they were further observed under SEM, as is shown in Fig. S2. It came out that the grain sizes of Mg-(0.5,1)Pr alloys were respectively $1.3 \pm 0.3 \,\mu m$ and $2.4 \pm 0.3 \,\mu m$. Thus, the grain refinement effect of proper Pr addition into Mg is prominent. Conversely, the addition of 1%Yb would coarsen the grains. It should be noted that the grain refinement and coarsening effects attributed greatly to the contents of Nd, Y and Yb. Changes on element contents could significantly alter the grain sizes of resulting Mg- (Nd, Y, Yb) binary alloys.

According to the optical microstructures shown in Fig. S1, the second phase could be observed in some binary Mg-RE alloys including Mg-(1,3)La, Mg-(1,3)Ce, Mg-(0.5,1,3)Pr, Mg-3Nd and Mg-(1,3) Eu alloys. As for the above Mg-RE alloys, the morphologies of the second phases were mostly in spherical or ribbonlike shape. It is obvious that the contents of the second phases increased with the REEs contents increased. Fig. 3 displays the XRD patterns of binary Mg-RE alloys as well as pure Mg for comparison. For convenience, the lower patterns in Fig. 3 were the alloys with single phases and the upper ones were with the second phases. The matrix phase of all experimental Mg-RE alloys was α -Mg. The presence of the second phase which could be judged from their microstructures was further verified by XRD patterns. Besides, the second phases of some other alloys (Mg-1Nd, Mg-(1,3)Sm, Mg-10Tm, Mg-3Yb and Mg-10Lu) were also detected. Among those Mg-RE alloys, the second phases were mostly composed of Mg₁₂RE (including Mg₁₂La, Mg₁₂Ce, Mg₁₂Pr, Mg₁₂Nd), which were all marked up by the same symbol. The phase constituents of 33 experimental Mg-RE alloys were listed in Table 1 in detail.

3.2. Mechanical property

The stress-strain curves of binary Mg-RE alloys and their mechanical properties are displayed in Fig. S3 and Fig. 4, respectively. For comparison, the data shown in histograms are all sorted from the lowest to the highest and the data of pure Mg is marked off for reference. According to these stress-strain curves, there was generally an inverse relationship between strength and ductility. In other words, the alloys with high strength always possessed low ductility and vice versa.

The experimental alloys could be roughly divided into two groups according to their stress-strain curve features: Group (I) alloys with high strength and low ductility, and Group (II) alloys with low strength and high ductility. These two types are plotted

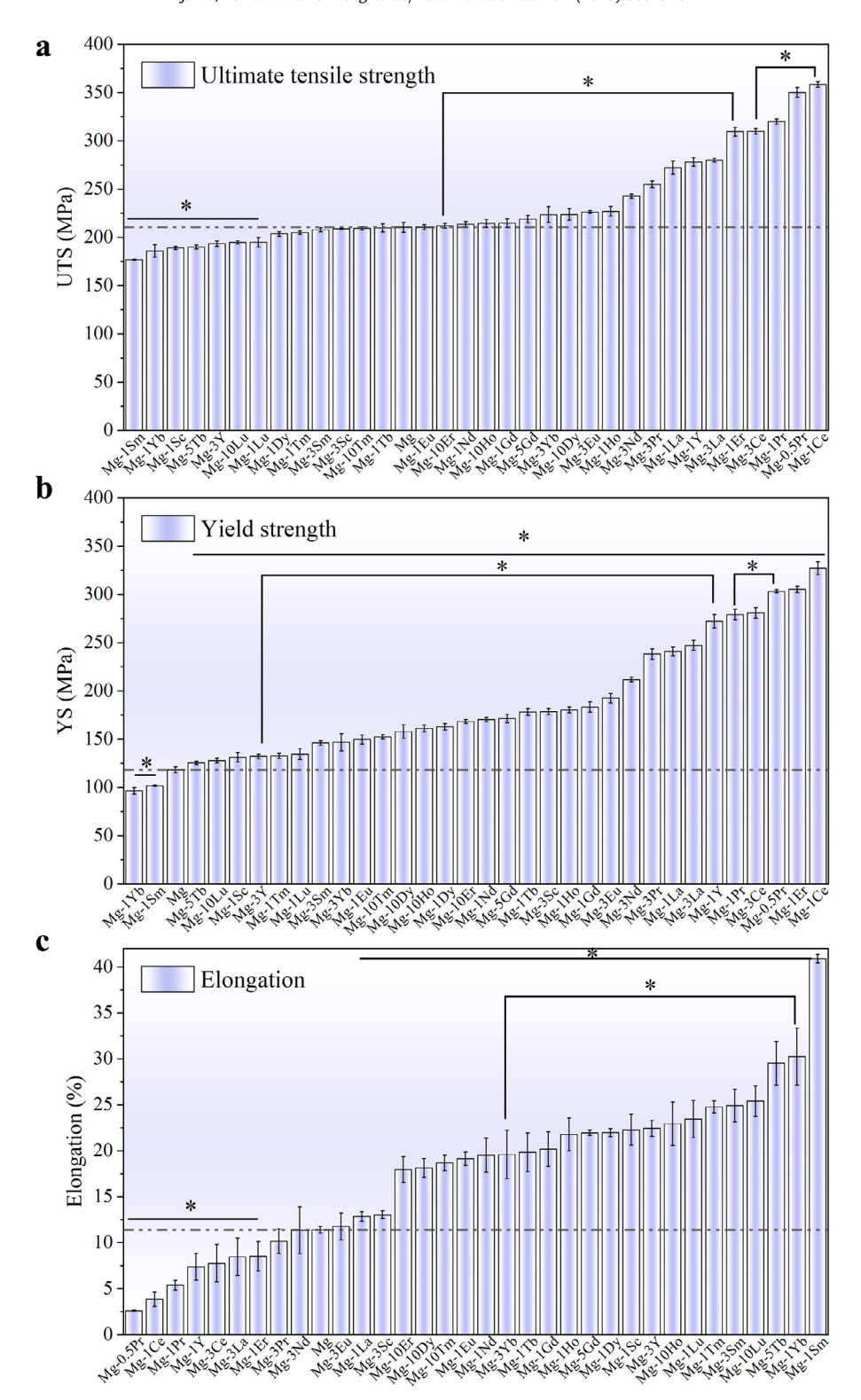


Fig. 4. Mechanical properties of experimental binary Mg-RE alloys and pure Mg. (a) ultimate tensile strength. (UTS) (b) yield strength (YS) (c) elongation at fracture.

separately in Fig. S3, in which (a) and (b) belong to the Group (I) while (c) (d) and (e) belong to Group (II). Among the Group (I), the addition of a small amount of elements Ce, Pr, Er and Y (1 wt.%) could effectively improve the strength of resulting Mg-RE alloys. But their UTS would decrease once the content of alloying elements increased to 3 wt.%. (As for Mg-Er alloy, the UTS decreased when Er content increased to 10 wt.%). Mg-1Ce exhibited the highest UTS and YS, which were $358 \pm 3 \text{ MPa}$ and $327 \pm 7 \text{ MPa}$,

respectively. Fig. 5 displays the typical fracture morphologies of experimental Mg-RE alloys and the overall view is shown in Fig. S4. Particularly, the fractures of Mg-1Ce and Mg-0.5Pr alloys which exhibited high strength and low ductility were relatively flat and showed brittle fracture features. For comparison, Pure Mg control group exhibited a typical cleavage fracture morphology with obvious cleavage steps and transgranular fracture features. As for Mg-RE alloys with low strength and high ductility, Mg-1Sm

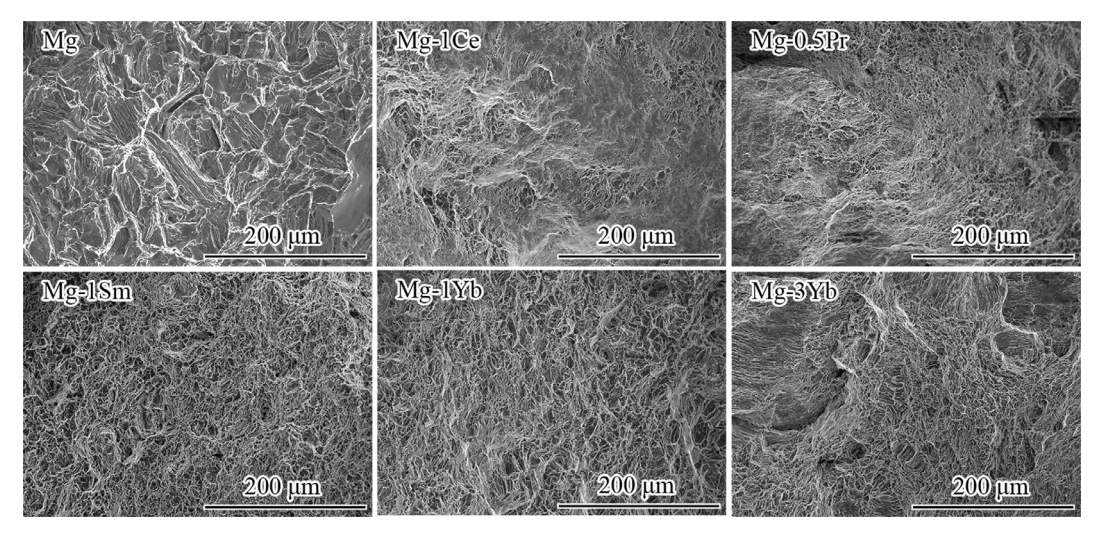


Fig. 5. Typical fracture morphologies of Mg-RE alloys and pure Mg.

and Mg-1Yb alloys showed high ductility. Further increase in alloying element's content (3 wt.%) would reduce their ductility but enhance their strength in the meantime. Among the experimental binary Mg-RE alloys, Mg-1Sm alloy possessed the highest elongation at fracture (40.9 \pm 0.5%). Correspondingly, the fracture morphology of Mg-1Sm alloy showed a typical pattern of ductile fracture. The tearing ridges were around the dimples, which were abundant on the fracture surface of Mg-1Sm alloy.

3.3. In vitro degradation test

3.3.1. Electrochemical evaluation

The OCP curves and potentiodynamic polarization curves of binary Mg-RE alloys are displayed in Fig. S5. Since some curves were similar, only the curves of four alloys with low corrosion rates (pure Mg, Mg-1Sc, Mg-3Pr, Mg-3Eu) and four with high corrosion rates (Mg-3Y, Mg-10Dy, Mg-1Er, Mg-10Lu) were shown. As for the OCP curves, all of the experimental Mg-RE alloys tended to be stable within a certain range. The OCP curves of the alloys with low corrosion rates were relatively smooth and stable. As for the alloys which exhibited high corrosion rate, the OCP curves were rough with comparatively wild and sharp fluctuations. This phenomenon was relative to the formation, rupture and re-formation of corrosion product layers [25,26]. According to the potentiodynamic polarization curves of Mg-RE alloys, the corrosion current densities could be calculated by Tafel extrapolation, as can be seen in Fig. 6. The OCP values and corrosion potentials of binary Mg-RE alloys and pure Mg are also displayed in Fig. 6. As can be expected, the OCP values and the corrosion potentials of alloys were similar. It is well known that the corrosion potential could reflect the tendency for corrosion. Lower corrosion potential generally indicates higher corrosion tendency. However, the actual corrosion rate should be determined by the corrosion current density since the degradation process is influenced by some other aspects such as the environmental factors and surface film conditions [27]. According to the corrosion current densities of binary Mg-RE alloys, Mg-3Eu was the only alloy whose corrosion rate was lower than that of pure Mg. Besides, the corrosion current densities of Mg-1Sm, Mg-3Sc, Mg-3Pr and Mg-1Sc alloys were comparatively low, indicating that these Mg-RE binary alloys possessed superior corrosion-resistant performance. By contrast, the Mg-RE alloys with high rare earth contents (Mg-10Ho, Mg-10Tm, Mg-10Dy, Mg-10Er and Mg-10Lu) exhibited inferior corrosion resistance.

3.3.2. Immersion test

During the immersion period, the pH values were recorded periodically. The pH change curves of experimental Mg-RE alloys and pure Mg are displayed in Fig. S6. As can be seen, the pH values of some Mg-RE alloys (Mg-(1,3) Sc, Mg-1Ce, Mg-(0.5,1) Pr, Mg-(1,3) Sm and Mg-1Eu) maintained lower than pure Mg during immersion period. While others were always higher than pure Mg, including Mg-3Y, Mg-10Dy, Mg-10Ho, Mg-(1,10) Er and Mg-10Tm. The pH values of the above alloys increased rapidly and exceeded 9.5 after only 72 h. In the later stage, the pH values tended to be comparatively steady. The pH values of experimental Mg-RE alloys after immersion for 72 h and 360 h are individually displayed in Fig. 7(a) and (b). Correspondingly, the corrosion rates of experimental Mg-RE alloys are displayed in Fig. 7(c) and (d), which were calculated by the weight loss after immersion for 72 h and 360 h, respectively. It should be noted that the increase of pH value would always lead to the decrease of corrosion rates. It is reported that as for magnesium alloys, the thickness of corrosion layer would increase with increasing pH value of solution and thus the layer would be more protective [28]. In that case, the corrosion rate would decrease to some extent. This opinion could also be confirmed by our results. As can be seen in Fig. 7, with immersion time prolonged, the pH values of Hank's solution increased and generally the corrosion rates of experimental Mg-RE alloys decreased to some extent. Besides, the corrosion rates of some Mg-RE alloys increased with higher RE content, including Mg-Sm, Mg-Ce, Mg-Y, Mg-Eu, Mg-Tm, Mg-Lu, Mg-Dy and Mg-Ho alloy systems. On the contrary, the corrosion rates of Mg-Gd and Mg-La alloys decreased with higher Gd/ La contents. According to Fig. 7(d), the corrosion rates of Mg-10Dy, Mg-10Ho, Mg-(1,10) Er and Mg-10Lu alloys were one order higher than the other Mg-RE alloys. On the whole, the corrosion resistance of Mg-light REE alloys was generally better than Mg-heavy REE alloys. It can be concluded that the proper addition of REEs -Sc, Pr, Sm, Eu (≤3 wt.%) would not damage the corrosion rate of magnesium.

The typical macroscopic morphologies of experimental Mg-RE alloys and pure Mg after immersion for 72 h and removal of corrosion product are displayed in Fig. 8 and the overall view are presented in Fig. S7. Mg-10Er alloy was severely corroded so it was difficult to discern its original morphology. As can be expected, corrosion pits were observed on pure Mg due to the attack of Cl⁻ in corrosion medium [29]. Besides, only a few Mg-RE alloys (Mg-(1,3) Sc, Mg-3Ce, Mg-3Nd and Mg-10Ho alloys) showed pitting corrosion while others exhibited filiform corrosion. To better

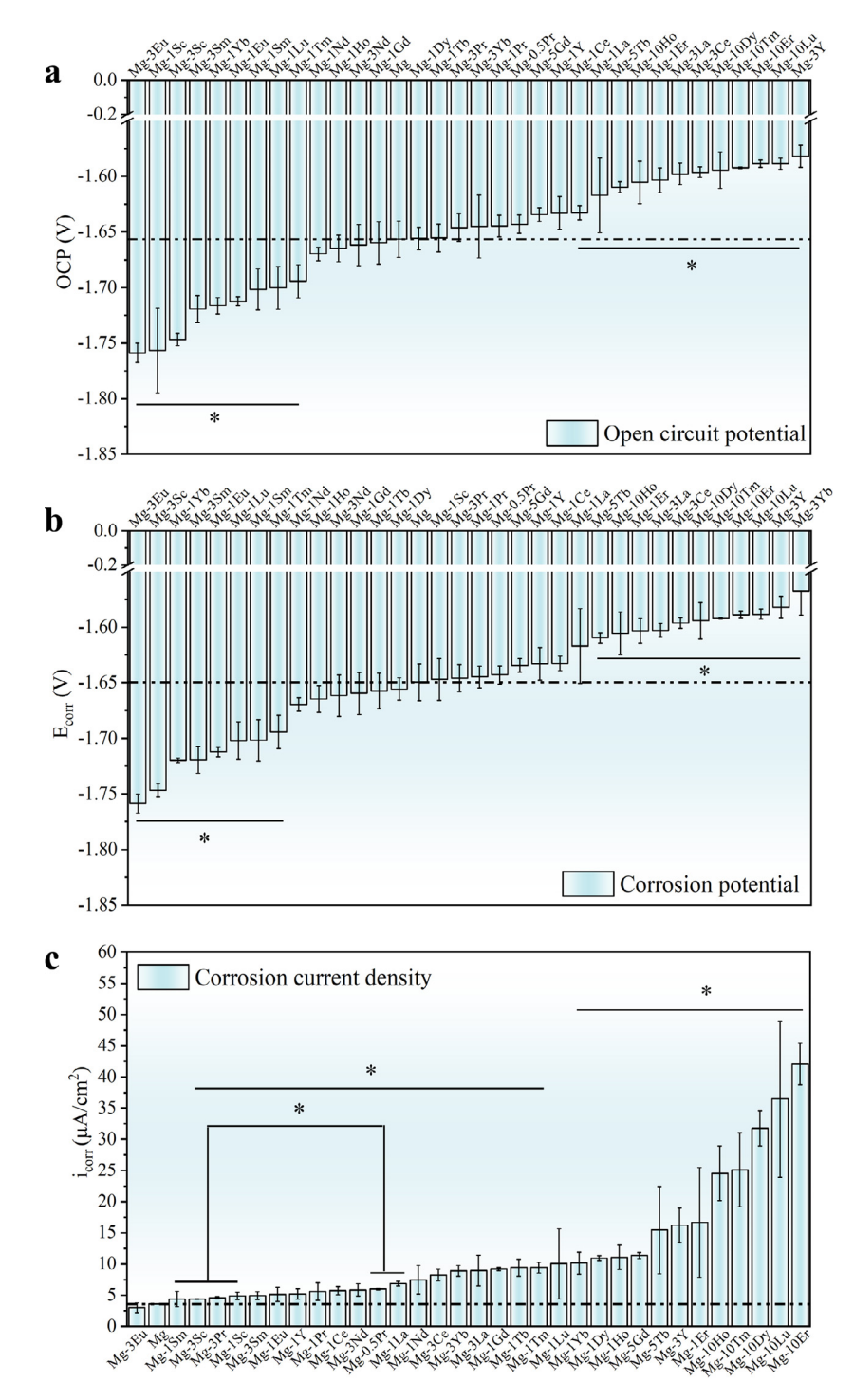


Fig. 6. Electrochemical test results of binary Mg-RE alloys and pure Mg. (a) open circuit potential. (OCP) (b) corrosion potential. (c) corrosion current density.

observe the corrosion pits on the above alloys, cross-sectional morphologies are shown in Fig. S8. It can be seen that the Mg-3Sc alloy exhibited a shallower corrosion pit than others, which is slightly less than 100 µm. While as for other alloys, the corrosion pits were deeper. Actually, there were many corrosion pits on each alloy yet it is hard to show them all. There were also some smaller corrosion pits on the alloys and the depth of which was merely several micrometers. The microscopic surface morphologies of Mg-RE alloys shown in Fig. S9 were in good correspondence with Fig. S7. Mg-10Er alloy displayed severe corrosion while several other alloys like Mg-1Sm alloy corroded slightly, which was similar

to pure Mg. After 360 h immersion, Mg-10(Dy, Ho, Lu) and Mg-1Er alloys degraded into fragments and thus their morphologies are not shown in Fig. S10 and Fig. S11. According to Fig. S10, unlike the surface morphology after 72 h immersion, pure Mg displayed relatively severe local corrosion after 360 h immersion. In comparison, some experimental Mg-RE alloys such as Mg-1Sc, Mg-1Ce and Mg-(1,3)Sm alloys only corroded slightly. As for the alloys containing heavy REEs (Y, Gd, Tb, Dy, Ho, Er, Tm, Yb, Lu), most of them were penetrated by aggressive ions in Hank's solution. Correspondingly, more corrosion products were observed on the surface of the above alloys in Fig. S11. According to the surface morphology

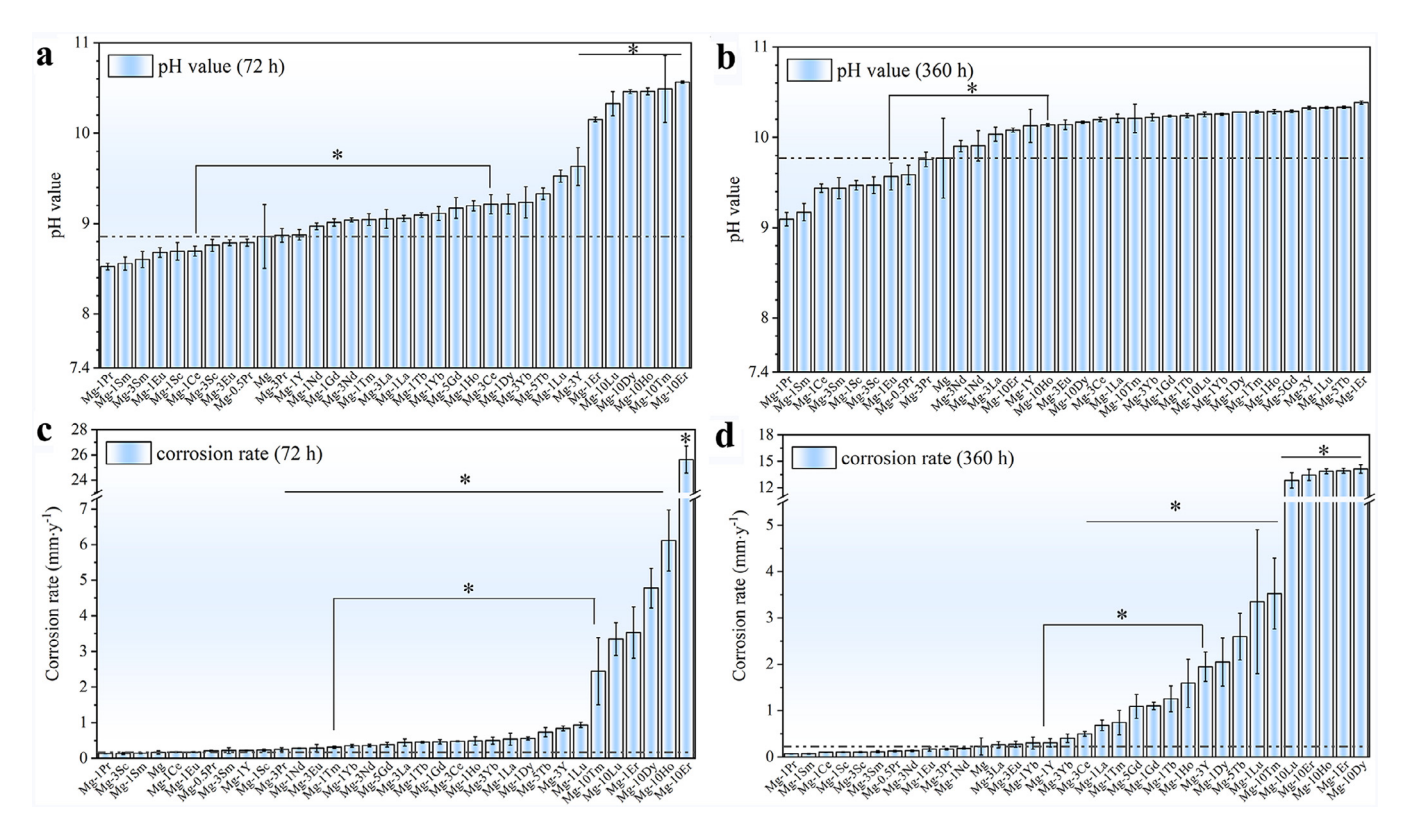


Fig. 7. pH values of Hank's solution after immersion for (a) 72 h (b) 360 h. The corrosion rates of Mg-RE model alloys and pure Mg after immersion for (a) 72 h (b) 360 h which is calculated by weight loss.

of Mg-1Lu alloy, the dense corrosion layer would be easy to be peeled off, leading to ions penetration and further corrosion.

Fig. 9 shows the element distribution on the cross-sectional of typical Mg-RE alloys after immersion. The element distribution of all experimental Mg-RE alloys is displayed in Fig. S12. The presence of REEs in corrosion layers was observed, especially for Mg-(1, 3)Sc, Mg-(1, 3)Y, Mg-10Er and Mg-10Tm alloys. In particular, the presence of element Y in the corrosion layer was more obvious than that in the matrix part for experimental Mg-Y alloys.

Fig. 10 displays the XRD patterns of the experimental Mg-RE alloys after immersion for 360 h. It can be seen that the corrosion products were mainly composed of Mg(OH)₂. CaCO₃ could also be detected in the corrosion products of Mg-1Dy alloy. Elements P and REEs were also detected by EDS, it can be conjectured that they were in small amounts and thus the corresponding products could not be revealed by XRD. In comparison with the XRD patterns of experimental alloys in Fig. 3, due to the presence of corrosion layers, the peaks derived from second phases in some of experimental Mg-RE alloys could hardly be discerned in Fig. 10.

3.4. Cytotoxicity

Fig. 11 presents the cytotoxicity of experimental Mg-RE alloy extracts. For convenience, the cell viabilities of MC3T3-E1 cells were plotted in order from the lowest to the highest. After culturing for 1 day, the cell viabilities of all experimental Mg-RE alloys were higher than 100% except for Mg-1Tm and Mg-3Yb alloys, whose cell viabilities were slightly lower than 100%. After culturing for 3 days, the cell viabilities decreased a little bit, but all of them were higher than 80%, which demonstrated that all experimental Mg-RE alloys were non-cytotoxic. Moreover, the cell viabilities of some Mg-RE alloys were higher than pure Mg and others were comparable, which preliminarily proved that proper addition

of REEs into magnesium would not cause toxic effect on MC3T3-E1 cells.

3.5. Hemocompatibility

Fig. 12 shows the hemolysis rates of binary Mg-RE alloys and pure Mg. Except for Mg-(1, 10)Lu alloys, all experimental binary Mg-RE alloys could meet the requirement of ISO 10,993–4, that is, their hemolysis rates were all lower than the judgment standard (5%). Moreover, the hemolysis rates of some alloys such as Mg-(1,3)Eu, Mg-(1, 10)Ho and Mg-(0.5, 1, 3)Pr alloys were lower than pure Mg. However, the addition of Lu into Mg could lead to serious hemolysis, especially when the content of Lu reached 10 wt.%. As for biodegradable magnesium alloy, hemolysis is caused by pH changes and ion release that alters the osmotic of liquid during the degradation process, which further destroys the erythrocyte [30]. It is supposed that the degradation rate of Mg-Lu alloy in PBS was fast, resulting in the rapid changes in pH and osmotic values and finally led to serious hemolysis.

Fig. 13, Fig. S13 and Fig. S14 displays the platelet adhesion of experimental Mg-RE alloys and pure Mg by SEM observation at low and high magnifications. According to Figs. 13 and S13, the platelet aggregation could be observed, if any. Compared with other alloys, the Mg-3Ce, Mg-0.5Pr and Mg-1Pr alloys exhibited more severe platelet aggregation. However, it should be noted that the experimental blood was from healthy rabbits, whose platelet concentration (about $1.487 \times 10^6 / \mu L$) is one order higher than healthy human bodies $(1.5 \times 10^5 - 4.5 \times 10^5 / \mu L)$ [31]. Therefore, it is supposed that such platelet aggregation would be mitigated when the alloys were applied to the blood environment of human bodies. Besides, although some platelets could be observed on Mg-(1, 3)Eu alloys, the distribution was relatively separated and no platelets aggregation was observed. As for other alloys, the number of platelets was fewer and the distribution was more scattered. On the sur-

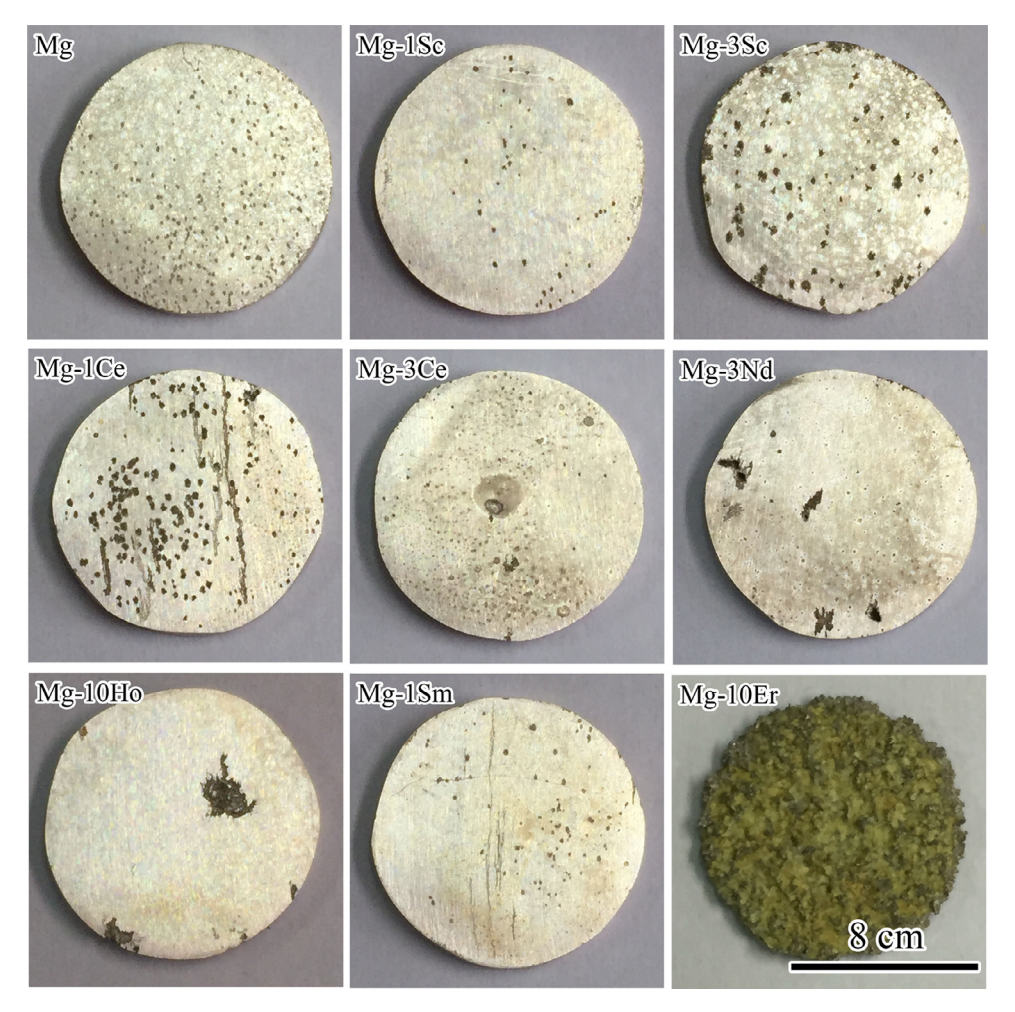


Fig. 8. Typical macroscopic surface morphologies of binary Mg-RE model alloys and pure Mg after immersion in Hank's solution for 72 h and removal of corrosion product.

face of Mg-10Lu alloy, no platelets but only corrosion products could be observed. It is supposed to be associated with the rapid degradation of Mg-10Lu alloy in such environment. According to Fig. S14, the morphological details of platelets on different Mg-RE alloys could be observed. It is known that the morphological changes of platelets could be divided into five stages: round, dendritic, spread-dendritic, spreading and fully spread, in correspondence with the activation level from un-activated to fully activated [32]. In this study, the platelets on most experimental alloys were spread-dendritic, corresponding to the activation level of partially activated. Besides, platelets on Mg-1Sc, Mg-3Y, Mg-3Ce, Mg-1Gd, Mg-10Dy and Mg-10Tm alloys were dendritic. It should be noted that sometimes the platelets on one alloy would not always be in the same stage. For example, partial platelets on Mg-3Sm, Mg-1Ho, Mg-1Er and Mg-1Tm alloys were spread-dendritic while others were spreading.

4. Discussion

4.1. Mechanical property, corrosion behavior and biocompatibility of binary Mg-RE alloy system

4.1.1. Mechanical property and corrosion behavior

In this study, the binary Mg-RE model alloys have been established in order to analyze the effect of individual REE on the performance of biomedical magnesium alloys. For comparison, pure Mg was adopted as a reference. Based on the ultimate tensile strength and elongation at fracture of pure Mg, the mechanical

properties of experimental Mg-RE alloys were summarized in an orthogonal coordinate system with pure Mg as the origin, as can be seen in Fig. 14. It is easy to comprehend that alloys in the first quadrant possessed higher mechanical properties than pure Mg, both in strength and ductility. These alloys were Mg-1La, Mg-3Eu, Mg-10Dy, Mg-10Er, Mg-1Nd, Mg-3Yb, Mg-(1, 5) Gd and Mg-(1, 10) Ho. However, with the content of alloying elements varied, the mechanical behaviors of binary Mg-RE alloys were different. For example, comparing with Mg-1La alloy, Mg-3La possessed inferior ductility. In other words, the ductility of Mg-La alloy decreased with the content of La increased from 1 wt.% to 3 wt.%. The reason why the increasing La content would lead to the reduction of ductility has been explained in the previous report [33]. It is said that the addition of La results in the formation of the second phases which are coarse and brittle. It further induces the crack initiation and limited ductility. No alloys were in the third quadrant, which means that the strength and ductility of experimental Mg-RE alloys were not all inferior to pure Mg. As for the alloys in the first and second quadrants, the strength of these alloys could be improved by proper addition of REEs. The strengthening mechanisms are discussed as follows. As for the single-phased experimental Mg-RE alloys, they could be strengthened by solid solution and grain refinement. The difference in radius between the diffusive solute atoms and magnesium atoms could result in lattice distortion of magnesium, which further leads to the increased resistance for dislocation movement and acts as solid solution strengthening. Since grain boundaries play a dominant role in hindering deformation, the strength increases with grain boundaries increase,

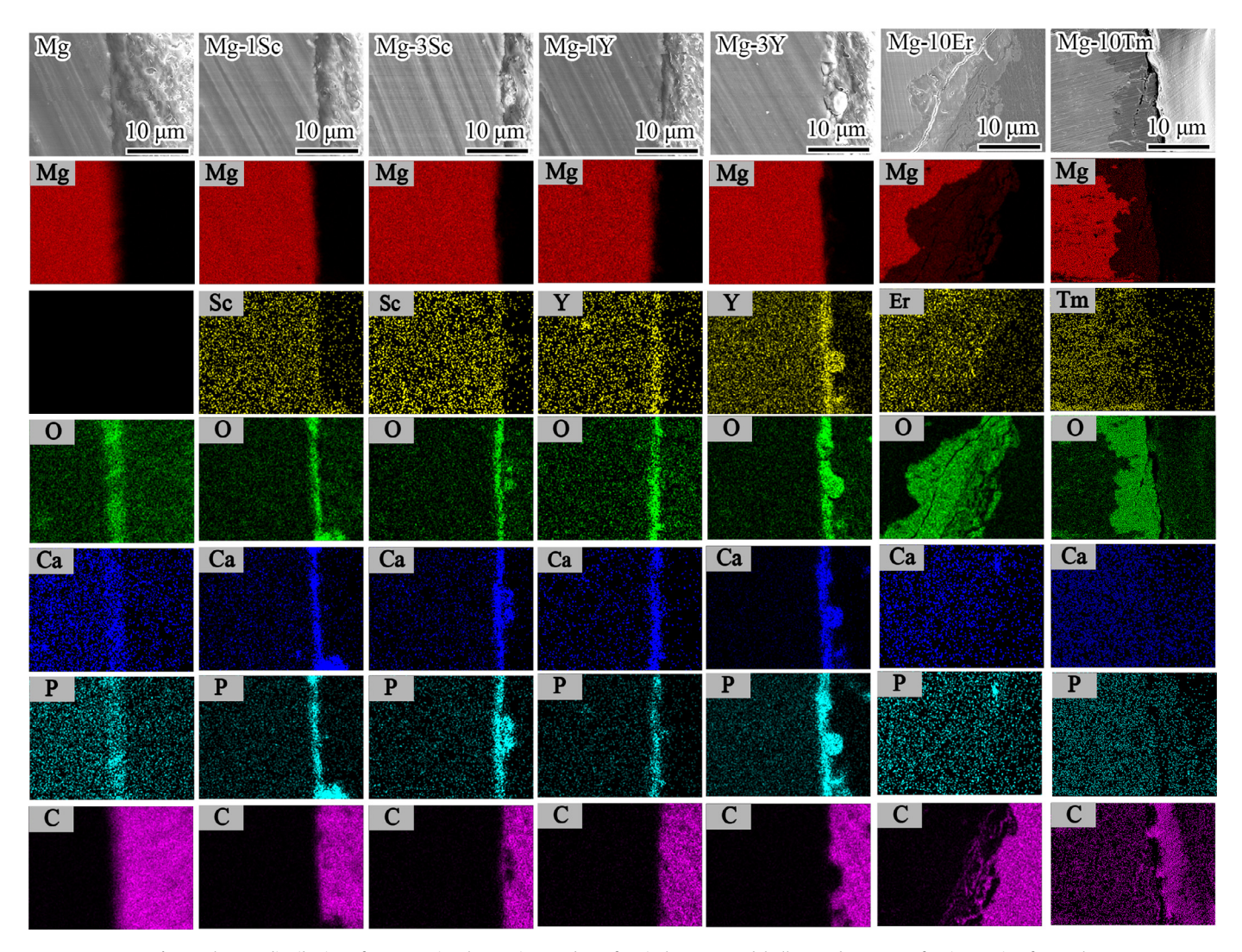


Fig. 9. Element distribution of cross-sectional corrosion product of typical Mg-RE model alloys and pure Mg after immersion for 360 h.

which is called grain refinement strengthening. For example, both the Mg-1Er and Mg-1Y are single-phased alloys. The yield strength of Mg-1Er alloy was higher than Mg-1Y alloy, which were respectively 305 ± 3 MPa and 272 ± 7 MPa. However, the grain size of the former $(7.3 \pm 0.8 \,\mu\text{m})$ was larger than the latter $(3.4 \pm 0.4 \,\mu\text{m})$. So, the grain refinement strengthening effect of Mg-1Y alloy is supposed to be more effective. And the reason for lower strength of Mg-1Y alloy should be attributed to the contribution of solidsolution strengthening. Since the atom radius of Er (232 pm) is larger than Mg (173 pm) while that of Y (180 pm) is similar to Mg, the solid-solution strengthening effect of Mg-1Er alloy would be more significant. With regard to the alloys with the second phases, the presence of the second phases could prevent the movement of dislocations and strengthen the alloys. Taken Mg-(0.5,1)Pr alloys as an example, the second phase were detected in both alloys. And the amount of the second phase in Mg-1Pr alloy should be higher than in Mg-0.5Pr alloy. Thus, the strengthening effect of the second phase in Mg-1Pr alloy should be more prominent. However, the yield strength of Mg-0.5Pr alloy (303 \pm 2 MPa) was higher than Mg-1Pr alloy (279 \pm 5 MPa). It should be attributed to the contribution of grain refinement strengthening since the grain size of Mg-0.5Pr alloy $(1.3 \pm 0.3 \,\mu\text{m})$ was finer than Mg-1Pr alloy $(2.4 \pm 0.3 \,\mu\text{m})$.

Binary Mg-RE alloys are the basis for the development of novel rare-earth-containing magnesium alloys and additional alloying elements could change the picture. Fig. S15 displays the mechani-

cal properties of binary Mg-RE and multicomponent Mg-RE based alloys. The former are derived from this study and the latter are summarized from other studies. For contrast, all alloys are asextruded. It can be seen that for multicomponent Mg-RE based alloys, Gd, Y, Nd, Er and Ce are the commonly-used REEs as alloying elements of magnesium. As can be seen in Fig. S15, both strength and ductility of binary Mg-RE alloys (in pink) could be improved by adding other alloying elements. Although the strength and ductility of binary Mg-RE alloys were in wide ranges, respectively from 176 to 358 MPa and 2.6% to 40.9%, the overall tendency is that the strength of one specific alloy is always inversely proportional to its ductility. For instance, Mg-1Ce alloy is of high strength and seems to be suitable for orthopedic implants, yet its inferior ductility limits its application. According to Fig. S15, the ductility of Mg-1Ce based alloy could be improved by adding proper Zn, Sn or Zr (Mg-4Zn-5Sn-1Ce, Mg-6Zn-0.5Zr-1Ce). Similarly, after adding Y and Zn into Mg-1Er alloy (Mg-1.5Zn-0.6Zr-1Er), both strength and ductility have been improved. As for Mg-Gd based alloys (Mg-6Gd-2Nd-0.5Zr, Mg-11Gd-1Zn, Mg-10Gd-2Y-0.5Zr, etc.), their mechanical properties get improved when compared with binary Mg-Gd alloys. Therefore, the addition of other alloying elements such as Zn, Zr and some REEs could improve the mechanical properties of Mg-Gd alloy substantially. With regard to Mg-Y based alloys, the addition of Sn (Mg-1Sn-3Y) and Zn (Mg-14.4Zn-3.3Y) would decrease their ductility but strengthen the alloys. Besides, the addition of

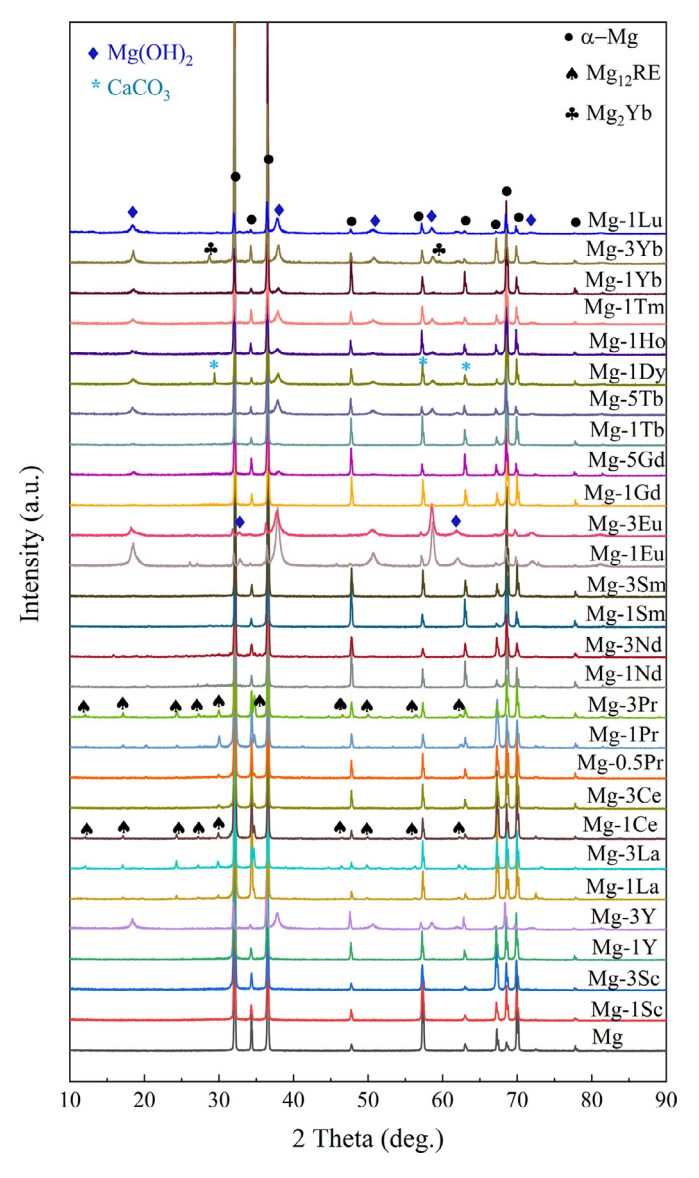


Fig. 10. XRD patterns of binary Mg-RE model alloys after immersion in Hank's solution for 360 h. Several alloys (Mg-10Dy, Mg-10Ho, Mg-1Er, Mg-10Er, Mg-10Lu) are excluded since they degraded into fragments after immersion for 360 h.

Zn and Zr (Mg-2.7Nd-0.2Zn-0.4Zr) could improve the strength of Mg-Nd alloy. However, it should be noted that although the processing state of all alloys shown in Fig. S15 is as-extruded, the mechanical properties of these alloys still exhibit limited comparability, which is due to the difference in the specific extrusion and heat-treatment parameters. Besides, after the addition of other alloying elements into binary Mg-RE alloys, the solid solubilities, microstructures as well as the phase compositions of alloys would be different, all of which are the essential reasons for the changes of their mechanical properties [34]. Taken the Mg-6Zn-xEr alloys as an example, it is reported that the *I*-phase and *W*-phase could be observed as the secondary phases [35]. The phase compositions of Mg-6Zn-xEr alloys would be different with the content of Er varies. In fact, the presence of W-phase and I-phase would have an impact on the mechanical properties of Mg-6Zn-xEr alloys. It is related to the face-centered cubic structure of the W-phase which would weaken the strength of the alloys and the close inherent interface between *I*-phase and α -Mg which would improve their strength. It should be noted that such phases could always be observed in some ternary rare-earth-containing phases but not in binary MgRE alloys [35]. Therefore, for future multicomponent alloy design, it is recommended to investigate the influence of adding other alloying elements on the microstructure changes of Mg-RE based alloys. It would help us to further study the internal mechanisms of their mechanical behaviors. With regard to the cardiovascular stent, superior plastic deformation ability and moderate strength of magnesium alloy are required so that during the expansion process the stent could be strengthened but not broken. Accordingly, Mg-1Sm alloy with ductility of 40.9% seems to be an ideal candidate for the cardiovascular stent, yet the strength needs to be improved further. Until now, the studies on the addition of Sm into biodegradable magnesium alloy is scarce. It is recommended that the strengthening elements such as Zn and Ce should be added in Mg-1Sm alloy for further study.

It is reported that in some Mg-RE-Zn systems (RE=Y, Gd, Tb, Dy, Ho, Er, Tm) various novel long period stacking ordered (LPSO) structure have been observed [36–38]. As for Mg-RE-Zn alloys with LPSO structure, both the plasticity and toughness would be excellent [5]. This is one of the reasons why Zn is a commonly-used alloying element of Mg-RE based alloys.

In addition, it is believed that the LPSO structure has an impact on the corrosion resistance of magnesium alloy. For example, after immersion in simulated body fluid (SBF) for 240 h, the mechanical properties of Mg-Y-Er-Zn alloy with LPSO structure could be maintained at a high level without much reduction [39]. As for the corrosion resistance of Mg-RE alloys, it is reported that REEs could incorporate into the corrosion products and protect the matrix from further corrosion [13,17], which has also been verified by our study. As is shown in Fig. 9, for both Mg-(1, 3)Sc alloys, Sc was detected not only in alloy matrix but also in corrosion layers. Similar conclusions can be drawn with regard to other binary Mg-RE alloys such as Mg-Y, Mg-Er and Mg-Tm alloys. It is believed that the presence of REEs in corrosion layers is always in the form of their oxides or hydroxides [13,17]. Since the Pilling-Bedworth ratios (PBR) of their oxides (Y₂O₃, Er₂O₃, Tm₂O₃ and Sc₂O₃) are slightly greater than 1, it is considered that the oxides are compact and their presence would improve the corrosion resistance of Mg-RE alloys to some extent. However, the corrosion behaviors of magnesium alloys are influenced by various aspects, so it is reasonable for some alloys to possess inferior corrosion resistance even though the PBR values of their REE oxides are slightly higher than 1.Taken Mg-(1,3)Y alloys as an example, although both of them are single-phased alloys, the corrosion rate increased largely from 0.30 ± 0.09 mm·y⁻¹ to 1.9 ± 0.3 mm·y⁻¹ with the content of yttrium increased. In that case, the influence of grain size on corrosion behavior should be considered. According to Fig. 2, the grain size of Mg-1Y alloy was merely $3.4 \pm 0.4 \mu m$ while the grain size of Mg-3Y alloy was much larger, which is $10\pm3\,\mu m$. In previous report, the effect of grain size on the corrosion behaviors of magnesium alloys has been evaluated [40]. It came out that the corrosion current density of pure magnesium had a linear increase with the logarithm of increasing grain size. In other words, pure magnesium with smaller grain size is supposed to possess higher corrosion resistance. This opinion has also been proved by other reports [41,42]. Hence, as for the Mg-3Y alloy in our experiment, the decreased corrosion resistance should be related to the increased grain size.

The explanation for how the grain size of alloy influence its corrosion resistance is given as below. It is relative to the PBR value of alloys. It is known that the PBR value of MgO is merely 0.81, which is caused by the discontinuity between the crystal structures of the oxide layer and magnesium alloy [43]. Thus, high compressive stress is present in the internal oxide layer. In order to reduce the mismatch and disorder between the oxide layer and alloy, one way is to introduce large volume fraction of grain boundaries per unit area [43]. That is, by refining the grains of alloy, the PBR value

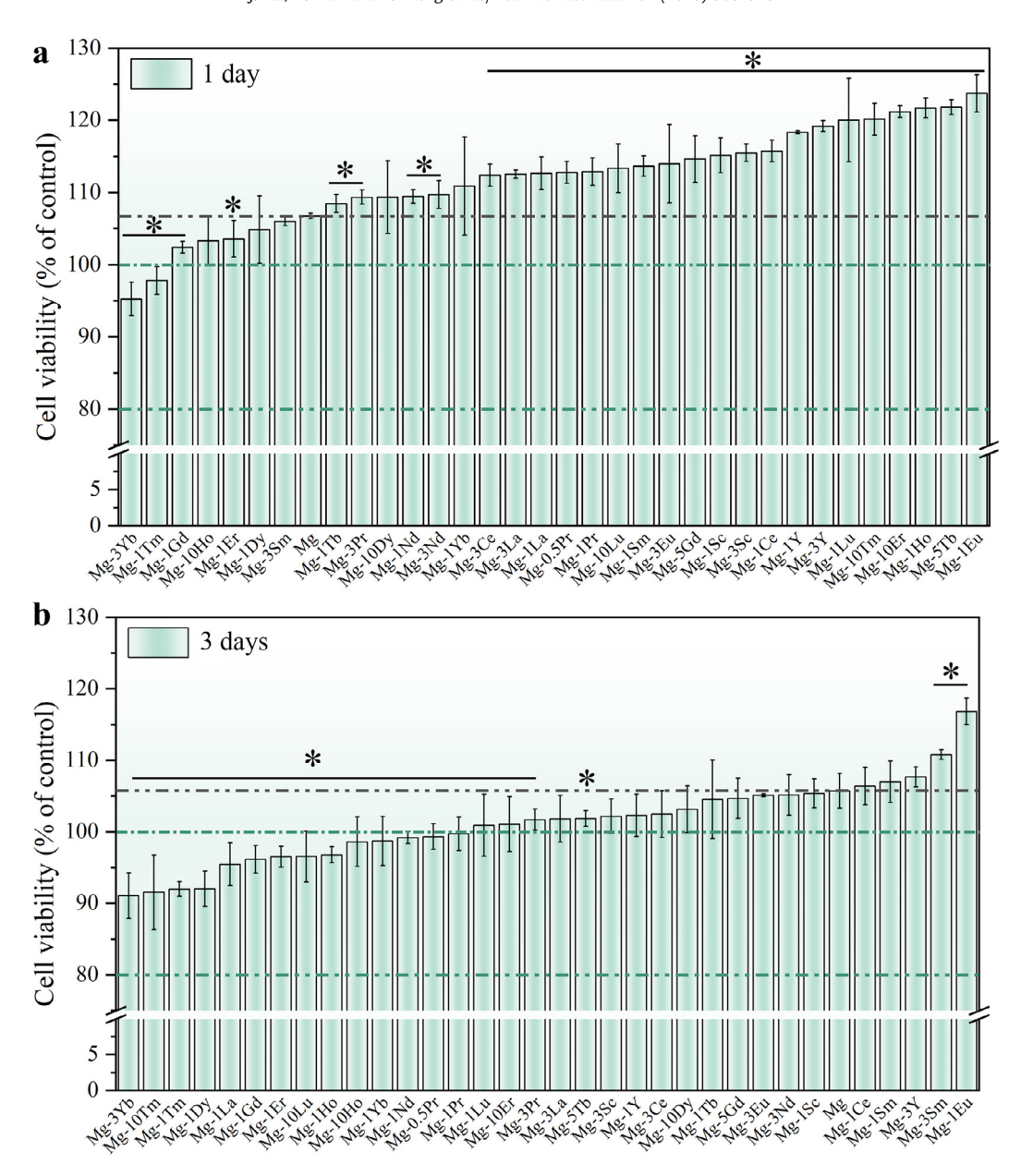


Fig. 11. Cell viabilities of MC3T3-E1 in binary Mg-RE model alloys and pure Mg extracts. (a) 1 day (b) 3 days.

of magnesium alloy could be increased and thus their corrosion resistance could be improved.

4.1.2. Biocompatibility

In our study, the cytotoxicity results have shown that all experimental Mg-RE alloys exhibited no toxic effect on MC3T3-E1 cells. However, it does not mean that the presence of REEs would not cause any adverse effect on cells. For example, it has been reported that the metabolic activity of human vascular smooth muscle cells (SMCs) was related to the concentration of RECl₃. Although the metabolic activity of SMCs did not change significantly over a wide concentration range, at high concentrations of RECl₃ it decreased, which was related to the incubation time with RECl₃ [44]. Besides, the upregulation of inflammatory genes has been induced due to the presence of REEs. As for another report concerning about the cytocompatibility of REEs, the effect of RECl₃ (RE=Y, Nd, Dy, Pr, Gd, La, Ce and Eu) with various concentrations on MG63, human umbilical cord perivascular (HUCPV) and RAW 264.7 cells has been studied comparatively, mainly focused on cytotoxicity, induction

of apoptosis and expression of inflammatory factors [45]. The results have shown that La and Ce exhibited the highest cytotoxicity among the REEs. As for elements with high solubility in Mg, elements Dy and Gd would be more appropriate as alloying elements of Mg than Y. As for elements with low solubility, the addition of elements Eu, Nd and Pr would be suitable in terms of biocompatibility.

Although several investigations on the in vitro cytocompatibility of REEs have been carried out, whether the in vitro results would be consistent with the *in vivo* environment still needs to be verified. According to the previous report, in a few cases, the results might be inconsistent. For example, it has been found that the Mg-1.27Ce alloy extracts showed cytotoxic effect on MC3T3-E1 even after 10 times dilution. However, no harmful effect has been shown after the implantation of Mg-Ce alloy in rabbits [16]. Besides, the *in vitro* test of Mg-10Gd alloy exhibited superior corrosion resistance (0.56 mm•y⁻¹) and no cytotoxic effect, while the *in vivo* test has revealed the rapid degradation of Mg-10Gd alloy, which damaged the bone remodeling process and caused

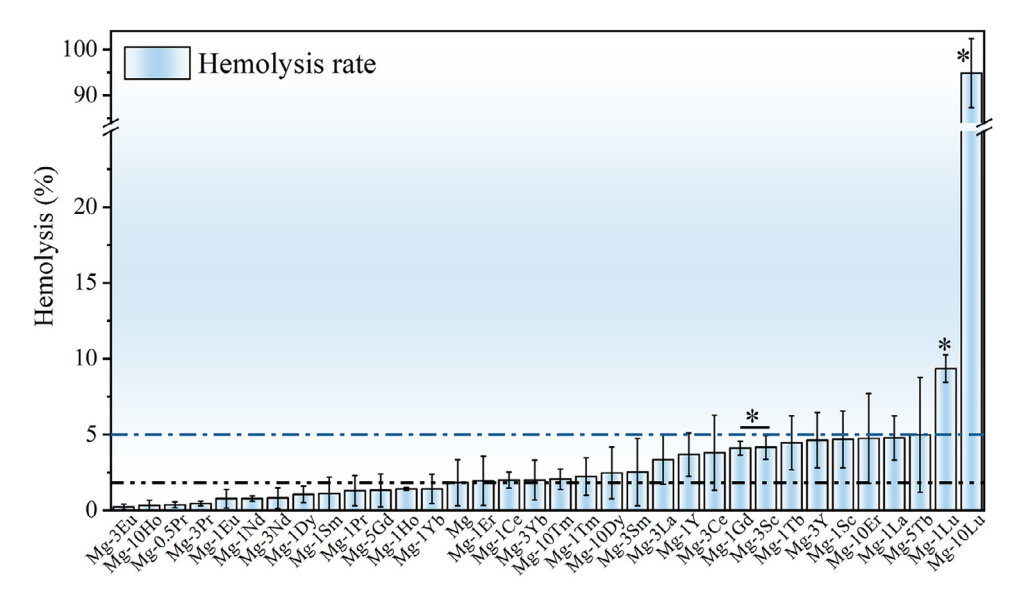


Fig. 12. Hemolysis rates of binary Mg-RE model alloys and pure Mg.

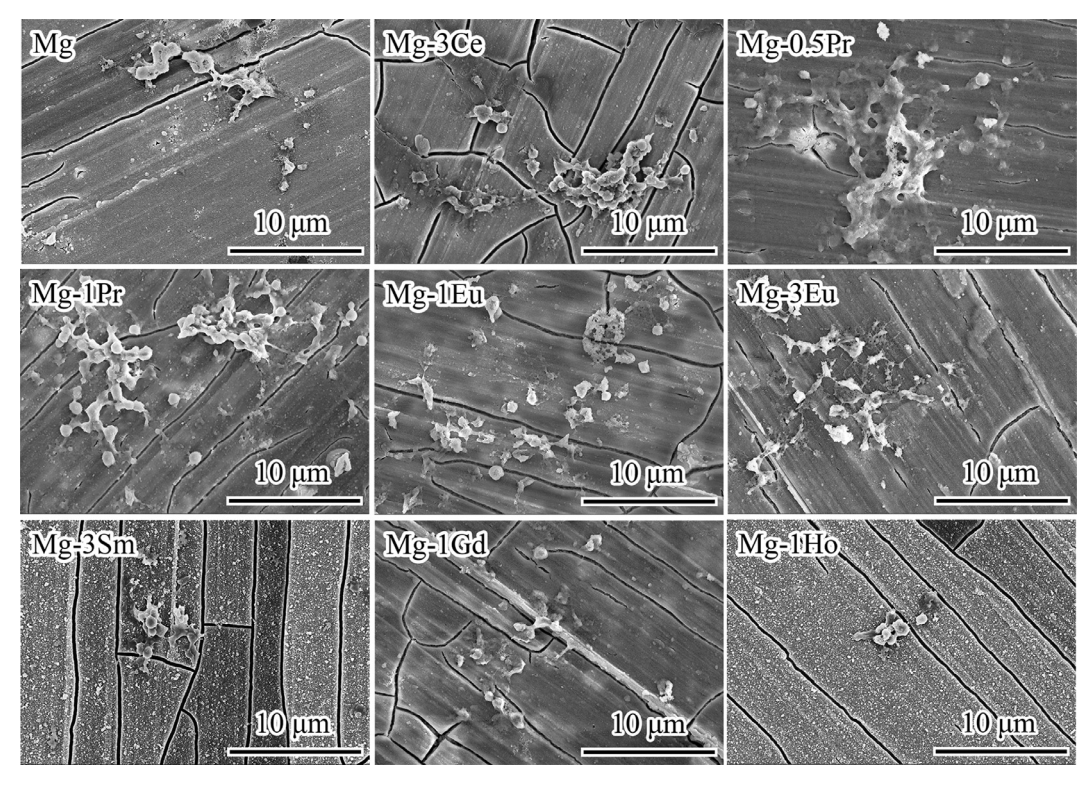


Fig. 13. Typical platelet adhesion of Mg-RE model alloys and pure Mg in low magnification under SEM.

the accumulation of Gd³⁺ in organs [46]. Although it is mentioned that the mechanical properties of binary Mg-Gd alloy could be further improved by adding other alloying elements, the biomedical application of Mg-Gd alloy still needs to be cautious since the accumulation of Gd *in vivo*. Besides, according to our own results, the Mg-(1,5) Gd alloys possessed good combination of strength and ductility. However, the inferior corrosion resistance would lead to the over-rapid release of Gd³⁺ and limits its application, which is in good correspondence to the previous report [46]. However, in some other reports, the *in vitro* and *in vivo* studies of magnesium alloys are comparable [47,48]. Thus, it is still meaningful to carry out the *in vitro* test for preliminary screening of magnesium alloys. Besides, it is reported that with prolonged immersion/ implanta-

tion period, the *in vitro* and *in vivo* test become more comparable [47]. So, it is suggested to extend the immersion period to better predict the actual behaviors of magnesium alloys *in vivo*.

Although the above-mentioned reports are mainly focused on the adverse effect of REEs, it does not imply the unpromising prospect of Mg-RE application. In fact, the rare-earth-containing magnesium alloy—WE43 alloy, has been optimized and implanted into the human body as bone screws or vascular stents for clinical study. The results are inspiring [49,50]. For example, as for the drug-eluting absorbable magnesium scaffold (DREAMS 2G), no stent thrombosis has been found after 6-month implantation. The target lesion failure was merely 3% and the myocardial infarction probability was less than 1% at 6 months, indicating that the

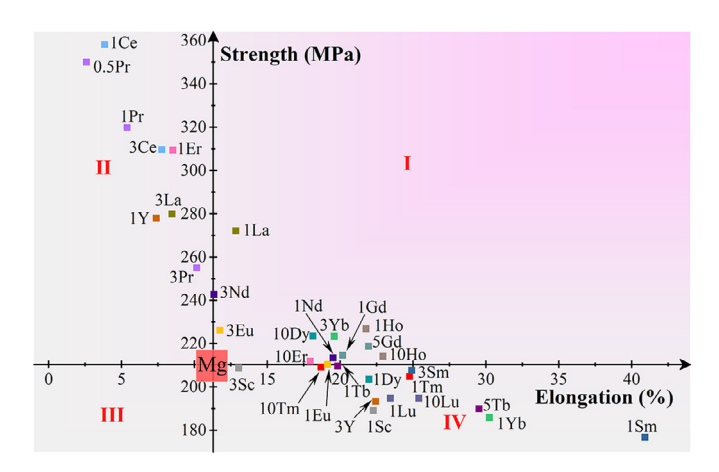


Fig. 14. Summary of the mechanical properties of experimental Mg-RE model alloys. (Pure Mg was selected as the reference.) For convenience, the "Mg-x RE alloys" is abbreviated as "x RE". For example, the "Mg-1Sc alloy" is expressed as "1Sc".

DREAMS 2 G could be an ideal alternative to present absorbable polymeric scaffolds [50].

As for an ideal biodegradable implant, good biocompatibility is necessary and additional new biofunction would be better. In actual, there have been several reports on the anticancer effect of REES [51–54]. For instance, it is reported that LaCl₃ and CeCl₃ could effectively inhibit the growth of leukemic cells and induce apoptosis. And with respect to LaCl₃ at low concentrations, no significant effect has been observed on normal bone marrow progenitor cells.

Moreover, the reports on toxicity, biological effects of REEs and their accumulation in organisms were summarized in Table 2, which could provide guidance for the element selection and composition design of biomedical Mg-RE alloys.

4.2. Perspectives on alloy design and development of biodegradable Mg-RE alloys

Biocompatibility and biodegradability are two necessary and sufficient conditions for alloying elements screening of biomedical magnesium alloys [27]. With regard to biocompatibility, Mg-Lu alloy showed serious hemolysis and its biomedical application is not suggested, especially for the cardiovascular field. As for biodegradability, several rare-earth-containing (Dy, Ho, Er, Lu) magnesium alloys exhibited rapid degradation rates (Fig. 7) and thus the adoption of these alloys for biomedical implants should also be cautious. The impurities in the above alloys should be strictly controlled. Besides, the addition of other alloying elements or surface modification methods are recommended to improve their corrosion resistance.

In consideration of the primary clinical applications of magnesium alloys, the remaining elements could be divided into two groups—alloys for cardiovascular and for orthopedic fields. As for the former, the addition of elements Sc, Nd, Sm, Eu, Gd, Tb, Tm and Yb into Mg could improve the ductility of alloys and would be preferable, especially Mg-1Sm and Mg-1Yb alloys, the ductility of which were higher than 30%. With regard to corrosion resistance, binary Mg-(Sc, Nd, Sm, Eu and Yb) alloys are preferable according to Fig. 7. In addition, it should be noted that animal tests have been carried out on Mg-(Sc, Nd, Gd) alloys and the accumulation of elements Nd and Gd in organs was reported [46,55]. Thus, the ion release of elements Nd and Gd in vivo should be controlled carefully.

As for alloys used for orthopedic implants, sufficient strength and mechanical integrity in early implantation period are essential to match the bone healing process. According to our mechanical results, the addition of elements Y, La, Ce and Pr into magnesium could effectively improve the strength of alloys. Among the above alloys, Mg-1Ce alloy showed the highest ultimate tensile strength of 358 ± 3 MPa. Mg-1Pr alloy showed the lowest corrosion rate of 0.069 ± 0.003 mm·y⁻¹. Animal test on the implantation of REEs (La, Ce, Pr) contained magnesium alloys showed that these rare earth ions were able to accumulate in liver, spleen, lung and kidney [55,56]. Therefore, the total content of REEs as well as the degradation rate of these magnesium alloys should be strictly controlled to avoid adverse effect on organisms.

To sum up, based on the comparative study of binary Mg-RE model alloys, we proposed the following research directions for the future developments of novel biomedical Mg-RE based alloys:

- (1) In vivo studies on binary Mg-RE model alloys; It is quite important to know how each rare earth element behaves inside the body after being released as the corrosion products of Mg-RE alloys. Can the rare earth element pass through or be metabolized/ assimilated by cells and/or tissue? According to LD₅₀ (mg·Kg⁻¹) data for the chlorides of rare earth elements obtained via intraperitoneal supplement of mouse [27], the sequence is Sc(755) > Nd(600) > Sm/Dy(585) >Ho(560) > Eu/Gd/Tb(550) > Er(535) > Tm(485) > Yb(395)> La(372.4) > Pr(358.9) > Ce(353.2) > Lu(315) > Y(88). It should be noted that element Y is one order of magnitude lower than all the other REEs, and should be cautious during usage. Some REEs have been found in the human body [95], including Ce (40 mg), La (no more than 1 mg), Y (0.5 mg), Sc (0.2 mg), and Sm (0.05 mg). For the REEs undetected in human body, we do not know whether it can be excreted outside of the body, or whether it was introduced into human body by food. For those REEs detected in the human body, whether it is good or harmful for the body is still unknown. Limited information can be found for the biosafety and biofunction of REEs (Sc, Y, La, Ce, Pr, Nd, Sm, Eu, Gd, Tb, Dy, Ho, Er, Tm, Yb and Lu) in animal model and human being model, and more work should be done. One key parameter is the content of rare earth element in excreta (urine and feces) after implantation into the animal model. If the rare earth element ions were detected in the excreta, it means that this kind of rare earth elements can be excreted. In principle, if the accumulation of REEs was found in the spleen, lung, liver and kidney, it might indicate an increased risk for chronic toxicity of REEs, and should be avoided.
- (2) Selection of "mischmetals" or single REE. It is recommended to add unspecific rare earth element with low dosage as the first choice. The target is to obtain single-phased solid solution with both solid-solution strengthening and grain refinement strengthening effects at the same time. Meanwhile the corrosion resistance could be kept by avoiding the precipitations of the secondary phase and the introduction of galvanic corrosion. For instance, we can add the REEs such as Gd and Ho, which both have high solid solubilities in Mg. Unfortunately, by simply adding these REEs, the strengths of binary Mg-RE alloys are generally below 300 MPa. Therefore, the best alloying strategy is to add both the REEs and other non-REEs elements into Mg, which is supposed to exhibit better strengthening effect. For example, multiple alloying with single REE and non-RE element Zn. Our recent work [96] have indicated that Mg-1.8Zn-0.2Gd alloy, composed of single α -Mg phase, owns excellent strength (UTS~300 MPa) and toughness that is comparable to the CE marked MAGNEZIX, the mischmetal added Mg alloy. Therefore, in order to develop biomedical Mg-RE based alloys with superior mechanical properties and corrosion resistance, while effectively avoid the possible chronic toxic effect of REEs, low addition of REEs, low total

Table 2Summary of the toxicity, biological effects of REEs and their accumulation in organisms.

Element	LD ₅₀ (i.p.) (mg•kg ⁻¹)	Biological effect	Accumulation in organism					
			model	Intake method	Observation time	Organ	Serum (Blood)	
Sc	755	It has been clinically used in the treatment of metastatic carcinomas with some success. The antibacterial and antifungal properties of Sc ³⁺ has been proved.	SD-rat	Implanted as Mg-30Sc in bone	24 weeks	No obvious accumulating tendency	Decreased after 24 weeks' implantation in serum	[17,57,58]
Y	88	Y ₂ O ₃ nanoparticle is reported to be neuroprotective, which protect nerve cells from oxidative stress. Animal test has shown that YCl ₃ could cause acute hepatic injury.	rat	IP injection of yttrium chloride	26 weeks	Accumulated in liver, spleen, lung and kidney.	N/A	[59–61]
La	372.4	LaCO ₃ is used for hyperphosphatemia treatment in renal failure and dialysis patients. While animal test has shown that the LaCl ₃ would impair memory.	German Black-headed mutton sheep	Implanted as LAE442 in bone	24 weeks	Significant higher content in liver and kidney	N/A	[56,62,63]
Ce	353.2	Nanoparticles of CeO ₂ is reported to be neuroprotective, which protect nerve cells from oxidative stress. Ce(NO ₃) ₃ could be used for antiseptic treatment for burns. But overdosage of Ce(NO ₃) ₃ could lead to toxicity and methemoglobinemia.	German Black-headed mutton sheep	Implanted as LAE442 in bone	24 weeks	Significant higher content in liver and kidney	N/A	[56,61,64]
Pr	358.9	The biological role is controversial. Pr is reported to protect liver cells by against phalloidin in vivo. But Pr could also cause hepatotoxic effects.	New-Zealand white rabbit	Implanted as LAE442 in bone	180 weeks	10–20 folds increased in liver, spleen, lung and kidney	N/A	[55,65,66]
Nd	600	Neodymium magnets are incorporated in medical devices such as magnetic resonance imaging device. However, the devices with neodymium magnets should be handled with great care. Nd could be used as anticoagulant for intravenous	New-Zealand white rabbit	Implanted as LAE442 in bone	180 weeks	10–20 folds increased in liver, spleen, lung and kidney	N/A	[55,65,67–69]
		injection. However, breathing the dust containing Nd and accumulated exposure could cause lung embolisms and liver damage, respectively.	New-Zealand white rabbit	Implanted as JDBM in common carotid artery	86 weeks	Increased at initial stage and later decreased to homeostatic level.	Below 0.1 ng/g all the time and was not detectable in blood	
Sm	585	Radioactive Sm-153 is used for cancer treatment and osteosarcoma. The intake of Sm(NO ₃) ₃ could cause pathological changes of organs, especially liver.	Wistar rat	IV injection of samarium chloride	6 days	Liver and skeleton showed higher take-up of Sm and the contents fell slowly with time.	Increased first and finally decreased to undetectable level	[70–72]
Eu	550	The clinical use of Eu is rare. An Eu DOTA-tetraamide complex could be used as an MRI sensor. The toxicity of Eu is mild according to various reports.	Wistar rat	gavage	4 weeks	One-hundred-thousandth of total dosed amount was found in liver, kidney, spleen and femurs.	N/A	[73–77]

(continued on next page)

Table 2 (continued)

Element	LD ₅₀ (i.p.) (mg•kg ⁻¹)	Biological effect	Accumulation in organism					
			model	Intake method	Observation time	Organ	Serum (Blood)	
Gd	550	Some Gd complexes are used as contrast agents in magnetic resonance imaging (MRI), which has been recently discovered to be relative to nephrotoxicity.	SD-rat	Implanted as Mg-10Gd in bone	36 weeks	Continuing increased Gd content in liver, spleen, lung and kidney.	No accumulation of Gd was detected in serum	[46,78]
Tb	550	The radioactive Tb element could be used for phantom studies and radiolabeling. Tb shows delayed acute toxicity and certain dosage of terbium chloride could suppress growth of mice.	Crj:ICR mice	IP injection of TbCl ₃	18-20 h	Higher in spleen, pancreas, and seminal vesicle. Lower in liver and testis.	N/A	[79–81]
Dy	585	Dy chelate complex could be applied as contrast agents for magnetic contrast imaging. The dysprosium shift reagents are proved to be nephrotoxic under 5 mM.	cat	IV injection of Dy-165 chelated with EDTA	1 h	Higher in lung and bone. Lower in liver and brain tissue.	The concentration in blood was lower 30 min after injection.	[82-84]
Но	560	Ho has been used as YAG surgical laser for applications such as laparoscopic partial nephrectomy. Ho shows delayed acute toxicity on cats.	Albino rat	Intramuscular injection of Holmium radioisotope in sodium citrate	1–8 days	56% of the injection dose was detected in bone. 2% was detected in liver.	N/A	[85–87]
Er	535	Er could be used as YAG in laser treatment such as YAG lithotripsy. It works more efficient than Ho: YAG in stone fragment. As for pharmacologic and toxicologic investigation, Er shows delayed acute toxicity, which is similar to Dy and Ho.	Albino rat	Intramuscular injection of Erbium radioisotope in sodium citrate	1–8 days	56% of the injection dosage was detected in bone and 1% was detected in liver.	N/A	[85,86,88]
Tm	485	Tm could be used as laser medium with high efficiency for nephrectomy, superficial ablation of tissue and so on. It could also be used as an X-ray source via brachytherapy for cancer treatment. Tm shows delayed acute toxicity and could cause the suppressed growth of rats.	Albino rat	Intramuscular injection of Thulium radioisotope in sodium citrate	1-8 days	64% of the injection dosage was detected in bone and 2%was detected in liver.	N/A	[80,85,89,90]
Yb	395	The radioisotope ¹⁷⁵ Yb has been used for palliative therapy of bone metastases as a tracer of polyaminophosphonates. YbF ₃ has been adopted as an inert and non-toxic tooth filling. Y shows delayed acute toxicity and might cause stomach hemorrhages, especially for females.	Wistar rat	IV injection of ytterbium chloride	6 days	Liver and skeletal showed higher take-up of Lu and the contents fell slowly with time	Increased first and finally decreased to a much lower level	[72,76,80,91]
Lu	315	The radionuclide of ¹⁷⁷ Lu can be used for both radioimmunotherapy and SPECT imaging. Lu could also be used as photodynamic therapy photosensitizers. LuCl ₃ acts as a depressant on system of organisms.	Albino rat	Intramuscular injection of Lutetium radioisotope in sodium citrate	1-8 days	68% of the injection dosage was detected in bone and 3% was detected in liver.	N/A	[92–94]

- content of alloying elements, multicomponent alloying by combining REEs and non-REEs are suggested for the future development of biomedical Mg-RE-based alloys.
- (3) Balance between precipitation hardening effect and matrixprecipitate galvanic corrosion. Except for solid solution strengthening and grain refinement strengthening, precipitation strengthening is believed to be another powerful strengthening method for magnesium alloys, even with the nano-size precipitates. Yet most of the secondary phases exhibit higher electrode potential than that of the α -Mg matrix phase. In that case, galvanic corrosion between the matrix and precipitate would be introduced. The α -Mg matrix phase would be depleted preferentially yet the precipitate would be left in the corrosion products. Thus, with regard to the presence of precipitate in the microstructure, basically the advantage is that the strength could be enhanced, while the disadvantage is that the corrosion products would be more difficult to pass through, to be metabolized/ assimilated by cells and/ or tissues. There is one exceptional second phase, Mg₂Ca, which have the electrode potential lower than that of α -Mg matrix phase [97], and it can be degraded preferentially before the biodegradation of α -Mg matrix phase. It might combine the advantage of both precipitation hardening effect and matrix-precipitate galvanic corrosion. Besides, if the distribution of the second phase is net-like and continuous, the presence of the second phase could also protect the matrix from corrosion even though the electrode potential of the second phase is higher than the matrix [9]. Therefore, it is important to manipulate the microstructure of alloys to balance the effect of the second phase on mechanical properties and corrosion behaviors of alloys.

5. Conclusions

In this work, a comparative study was carried out to investigate the individual effect of 16 REEs as micro-alloying elements of magnesium on their microstructures, mechanical properties, corrosion behaviors and biocompatibility. The results indicated that a wide range of mechanical properties could be achieved by adding different REEs into Mg. The incorporation of REEs (Sc, Y, Er, Tm) into corrosion layer was observed, which is supposed to improve the corrosion resistance of magnesium alloys. As for biocompatibility, no alloys showed toxicity on MC3T3-E1 cells, but the hemocompatibility of Mg-Lu alloys was not satisfactory.

In general, as alloying elements of Mg, the REEs (Y, La, Ce, Pr) are more suitable for orthopedic application while the REEs (Sc, Nd, Sm, Eu, Gd, Tb, Tm, Yb) are more suitable for the cardiovascular field. Moreover, to further develop the rare-earth-containing magnesium alloys with better integrated performance, the addition of other non-RE elements (e.g. Zn) is suggested.

Declaration of Competing Interest

The authors declare that they have no known competing financial interests or personal relationships that could have appeared to influence the work reported in this paper.

Acknowledgements

This work was supported by the National Key R&D Program of China (2018YFC1106600), National Natural Science Foundation of China (Grant No. 51871004 and 51431002) NSFC/RGC Joint Research Scheme (Grant No. 51661165014), and Peking University Medicine Seed Fund for Interdisciplinary Research (Grant No. BMU2018ME005).

Supplementary materials

Supplementary material associated with this article can be found, in the online version, at doi:10.1016/j.actbio.2019.11.013.

References

- [1] Nan Li, Yufeng Zheng, Novel magnesium alloys developed for biomedical application: a review, J. Mater. Sci. Technol. 29 (2013) 489–502.
- [2] Y.F. Zhang, J.K. Xu, Y.C. Ruan, M.K. Yu, M. O'Laughlin, H. Wise, D. Chen, L. Tian, D.F. Shi, J.L. Wang, S.H. Chen, J.Q. Feng, D.H.K. Chow, X.H. Xie, L.Z. Zheng, L. Huang, S. Huang, K.K. Leung, N. Lu, L. Zhao, H.F. Li, D.W. Zhao, X. Guo, K.M. Chan, F. Witte, H.C. Chan, Y.F. Zheng, L. Qin, Implant-derived magnesium induces local neuronal production of CGRP to improve bone-fracture healing in rats, Nat. Med. 22 (2016) 1160–1169.
- [3] Y. Zheng, X. Gu, F. Witte, Biodegradable metals, Mater. Sci. Eng. R Rep. 77 (2014) 1–34.
- [4] Y. Xin, T. Hu, P. Chu, In vitro studies of biomedical magnesium alloys in a simulated physiological environment: a review, Acta Biomater. 7 (4) (2011) 1452–1459.
- [5] Y. Chen, Z. Xu, C. Smith, J. Sankar, Recent advances on the development of magnesium alloys for biodegradable implants, Acta Biomater. 10 (11) (2014) 4561–4573.
- [6] X. Gu, Y. Zheng, Y. Cheng, S. Zhong, T. Xi, In vitro corrosion and biocompatibility of binary magnesium alloys, Biomaterials 30 (4) (2009) 484–498.
- [7] X. Gu, X. Xie, N. Li, Y. Zheng, L. Qin, In vitro and in vivo studies on a mg-sr binary alloy system developed as a new kind of biodegradable metal, Acta Biomater. 8 (6) (2012) 2360–2374.
- [8] S. Zhang, X. Zhang, C. Zhao, J. Li, Y. Song, C. Xie, H. Tao, Y. Zhang, Y. He, Y. Jiang, Y. Bian, Research on an mg-zn alloy as a degradable biomaterial, Acta Biomater. 6 (2) (2010) 626-640.
- [9] D. Bian, W. Zhou, J. Deng, Y. Liu, W. Li, X. Chu, P. Xiu, H. Cai, Y. Kou, B. Jiang, Development of magnesium-based biodegradable metals with dietary trace element germanium as orthopaedic implant applications, Acta Biomater. 64 (2017) 421.
- [10] J. Zheng, Q. Wang, Z. Jin, T. Peng, Effect of sm on the microstructure, mechanical properties and creep behavior of Mg-0.5Zn-0.4 Zr based alloys, Mater. Sci. Eng., A 527 (7-8) (2010) 1677-1685.
- [11] F. Mert, C. Blawert, K.U. Kainer, N. Hort, Influence of cerium additions on the corrosion behaviour of high pressure die cast AM50 alloy, Corros. Sci. 65 (2012) 145–151.
- [12] G. Song, A. Atrens, Understanding magnesium corrosion—a framework for improved alloy performance, Adv. Eng. Mater. 5 (12) (2003) 837–858.
- [13] W. Liu, F. Cao, L. Chang, Z. Zhang, J. Zhang, Effect of rare earth element ce and la on corrosion behavior of AM60 magnesium alloy, Corros. Sci. 51 (6) (2009) 1334–1343.
- [14] L. Yang, Y. Huang, F. Feyerabend, R. Willumeit, K.U. Kainer, N. Hort, Influence of ageing treatment on microstructure, mechanical and bio-corrosion properties of Mg-Dy alloys, J. Mech. Behav. Biomed. Mater. 13 (2012) 36-44.
- [15] N. Hort, Y. Huang, D. Fechner, M. Störmer, C. Blawert, F. Witte, C. Vogt, H. Drücker, R. Willumeit, K. Kainer, Magnesium alloys as implant materials-Principles of property design for Mg–RE alloys, Acta Biomater. 6 (5) (2010) 1714–1725.
- [16] E. Willbold, X. Gu, D. Albert, K. Kalla, K. Bobe, M. Brauneis, C. Janning, J. Nellesen, W. Czayka, W. Tillmann, Effect of the addition of low rare earth elements (lanthanum, neodymium, cerium) on the biodegradation and biocompatibility of magnesium, Acta Biomater. 11 (2015) 554–562.
- [17] J. Liu, Y. Lin, D. Bian, M. Wang, Z. Lin, X. Chu, W. Li, Y. Liu, Z. Shen, Y. Liu, Y. Tong, Z. Xu, Y. Zhang, Y. Zheng, *In vitro* and *in vivo* studies of Mg-30Sc alloys with different phase structure for potential usage within bone, Acta Biomater. 98 (2019) 50–66.
- [18] A. Saccone, A. Cardinale, S. Delfino, R. Ferro, A contribution to the rare earth intermetallic chemistry: praseodymium-magnesium alloy system, Intermetallics 1 (3) (1993) 151–158.
- [19] ASTM E112-13, Standard Test Methods for Determining Average Grain Size, annual book of ASTM standards, American Society for Testing and Materials, West Conshohocken, PA, 2013.
- [20] ASTM E8-04, Standard Test Methods for Tension Testing of Metallic Materials, annual book of ASTM standards, American Society for Testing and Materials, West Conshohocken, PA, 2004.
- [21] ASTM G102-89, Standard Practice for Calculation of Corrosion Rates and Related Information from Electrochemical Measurements, annual book of ASTM standards, American Society for Testing and Materials, West Conshohocken, PA, 2010.
- [22] ASTM G31-72, Standard Practice for Laboratory Immersion Corrosion Testing of Metals, annual book of ASTM standards, American Society for Testing and Materials, West Conshohocken, PA, 2004.
- [23] ASTM G1-90, Standard Practice for Preparing, Cleaning, and Evaluating Corrosion Test Specimens, annual book of ASTM standards, American Society for Testing and Materials, West Conshohocken, PA, 1999.
- [24] Z. Shi, M. Liu, A. Atrens, Measurement of the corrosion rate of magnesium alloys using tafel extrapolation, Corros. Sci. 52 (2) (2010) 579–588.
- [25] Y.S. Jiménez, M.T. Gil, M.T. Guerra, L. Baltes, J. Rosca, Interpretation of open circuit potential of two titanium alloys for a long time immersion in physiological fluid, Bull. Transil. Uni. Braşov 2 (2009) 51.

- [26] R.C. Zeng, Y. Hu, S.-K. Guan, H.-Z. Cui, E.-H. Han, Corrosion of magnesium alloy AZ31: the influence of bicarbonate, sulphate, hydrogen phosphate and dihydrogen phosphate ions in saline solution, Corros. Sci. 86 (2014) 171–182.
- [27] Y. Liu, Y. Zheng, X.H. Chen, J.A. Yang, H. Pan, D. Chen, L. Wang, J. Zhang, D. Zhu, S. Wu, Fundamental theory of biodegradable metals—definition, criteria, and design, Adv. Funct. Mater. 29 (2019) 1805402.
- [28] S. Johnston, Z. Shi, A. Atrens, The influence of pH on the corrosion rate of high-purity mg, AZ91 and ZE41 in bicarbonate buffered hanks' solution, Corros. Sci. 101 (2015) 182–192.
- [29] Y. Xin, K. Huo, H. Tao, G. Tang, P.K. Chu, Influence of aggressive ions on the degradation behavior of biomedical magnesium alloy in physiological environment. Acta Biomater. 4 (6) (2008).
- [30] M. Jacobs, A.K. Parpart, Osmotic properties of the erythrocyte: II. the influence of pH, temperature, and oxygen tension on hemolysis by hypotonic solutions, Biol. Bull. 60 (2) (1931) 95–119.
- [31] E.-S. Kim, E.J. Park, P.H. Choung, Platelet concentration and its effect on bone formation in calvarial defects: an experimental study in rabbits, J. Prosthet. Dent. 86 (4) (2001) 428–433.
- [32] T.M. Ko, S.L. Cooper, Surface properties and platelet adhesion characteristics of acrylic acid and allylamine plasma-treated polyethylene, J. Appl. Polym. Sci. 47 (9) (1993) 1601–1619.
- [33] P. Maier, M. Bechly, C. Mendis, N. Hort, Precipitation hardening on mechanical and corrosion properties of extruded Mg10Gd modified with ND and LA, Metals (Basel) 8 (8) (2018) 640.
- [34] R. Wu, Z. Qu, M. Zhang, Reviews on the influences of alloying elements on the microstructure and mechanical properties of Mg–Li base alloys, Rev. Adv. Mater. Sci 24 (3) (2010) 35–43.
- [35] K. Liu, Q. Wang, W. Du, Z. Wang, S. Li, Microstructure and mechanical properties of extruded Mg-6Zn-Xer alloys, Trans. Nonferrous Met. Soc. China 23 (2013) 2863–2873.
- [36] P. Chen, D.L. Li, J.X. Yi, B.Y. Tang, L.M. Peng, W.J. Ding, Microstructure and electronic characteristics of the 6H-type abacab Lpso structure in Mg97Zn1Y2 alloy, J. Alloys Compd. 485 (1) (2009) 672–676.
- [37] M. Yamasaki, K. Hashimoto, K. Hagihara, Y. Kawamura, Effect of multimodal microstructure evolution on mechanical properties of Mg–Zn–Y extruded alloy, Acta Mater. 59 (9) (2011) 3646–3658.
- [38] T.W. Fan, B.Y. Tang, L.M. Peng, W.J. Ding, First-principles study of long-period stacking ordered-like multi-stacking fault structures in pure magnesium, Scripta Mater 64 (10) (2011) 942–945.
- [39] Z. Leng, J. Zhang, T. Yin, L. Zhang, X. Guo, Q. Peng, M. Zhang, R. Wu, Influence of biocorrosion on microstructure and mechanical properties of deformed mg-y-er-zn biomaterial containing 18R-LPSO phase, J. Mech. Behav. Biomed. Mater. 28 (2013) 332–339.
- [40] G. Argade, S. Panigrahi, R. Mishra, Effects of grain size on the corrosion resistance of wrought magnesium alloys containing neodymium, Corros. Sci. 58 (2012) 145–151.
- [41] C. op't Hoog, N. Birbilis, Y. Estrin, Corrosion of pure Mg as a function of grain size and processing route, Adv. Eng. Mater. 10 (6) (2008) 579–582.
- [42] N. Birbilis, M.X. Zhang, Y. Estrin, Surface grain size effects on the corrosion of magnesium, Key Eng. Mater. Trans Tech. Publ (2008) 229–240.
- [43] N. Birbilis, K.D. Ralston, S. Virtanen, H.L. Fraser, C.H.J. Davies, Grain character influences on corrosion of ECAPed pure magnesium, Corros. Eng. Sci. Techn. 45 (3) (2010) 224–230.
- [44] A. Drynda, N. Deinet, N. Braun, M. Peuster, Rare earth metals used in biodegradable magnesium-based stents do not interfere with proliferation of smooth muscle cells but do induce the upregulation of inflammatory genes, J. Biomed. Mater. Res. Part A 91 (2) (2009) 360–369.
- [45] F. Feyerabend, J. Fischer, J. Holtz, F. Witte, R. Willumeit, H. Drücker, C. Vogt, N. Hort, Evaluation of short-term effects of rare earth and other elements used in magnesium alloys on primary cells and cell lines, Acta Biomater. 6 (5) (2010) 1834–1842.
- [46] A. Myrissa, S. Braeuer, E. Martinelli, R. Willumeit-Römer, W. Goessler, A.M. Weinberg, Gadolinium accumulation in organs of sprague-dawley[®] rats after implantation of a biodegradable magnesium-gadolinium alloy, Acta Biomater. 48 (2017) 521–529.
- [47] A. Myrissa, N.A. Agha, Y. Lu, E. Martinelli, J. Eichler, G. Szakács, C. Kleinhans, R. Willumeit-Römer, U. Schäfer, A.-M. Weinberg, In vitro and in vivo comparison of binary Mg alloys and pure Mg, Mater. Sci. Eng., C 61 (2016) 865–874.
- [48] N.I. Zainal Abidin, B. Rolfe, H. Owen, J. Malisano, D. Martin, J. Hofstetter, P.J. Uggowitzer, A. Atrens, The *in vivo* and *in vitro* corrosion of high-purity magnesium and magnesium alloys WZ21 and AZ91, Corros. Sci. 75 (2013) 354–366.
- [49] H. Windhagen, K. Radtke, A. Weizbauer, J. Diekmann, Y. Noll, U. Kreimeyer, R. Schavan, C. Stukenborg-Colsman, H. Waizy, Biodegradable magnesium-based screw clinically equivalent to titanium screw in hallux valgus surgery: short term results of the first prospective, randomized, controlled clinical pilot study, Biomed. Eng. Online 12 (1) (2013) 62.
- [50] M. Haude, H. Ince, A. Abizaid, R. Toelg, P.A. Lemos, C. von Birgelen, E.H. Christiansen, W. Wijns, F.J. Neumann, C. Kaiser, Safety and performance of the second-generation drug-eluting absorbable metal scaffold in patients with de-novo coronary artery lesions (BIOSOLVE-II): 6 month results of a prospective, multicentre, non-randomised, first-in-man trial, Lancet North Am. Ed. 387 (10013) (2016) 31–39.
- [51] D. Magda, R.A. Miller, Motexafin gadolinium: a novel redox active drug for cancer therapy, Semin. Cancer Biol., Elsevier (2006) 466–476.

- [52] I. Kostova, G. Momekov, P. Stancheva, New samarium (III), gadolinium (III), and dysprosium (III) complexes of coumarin-3-carboxylic acid as antiproliferative agents, Met. Based Drugs 2007 (2007).
- [53] Y. Dai, J. Li, J. Li, L. Yu, G. Dai, A. Hu, L. Yuan, Z. Wen, Effects of rare earth compounds on growth and apoptosis of leukemic cell lines, In Vitro Cellular and Develop. Biol. Animal 38 (7) (2002) 373–375.
- [54] N. Anisimova, M. Kiselevskiy, N. Martynenko, B. Straumal, R. Willumeit-Römer, S. Dobatkin, Y. Estrin, Cytotoxicity of biodegradable magnesium alloy WE43 to tumor cells in vitro: bioresorbable implants with antitumor activity? J. Biomed. Mater. Res. Part B:Appl. Biomater. (2019).
- [55] N. Angrisani, J. Reifenrath, F. Zimmermann, R. Eifler, A. Meyer-Lindenberg, K. Vano-Herrera, C. Vogt, Biocompatibility and degradation of LAE442-based magnesium alloys after implantation of up to 3.5years in a rabbit model, Acta Biomater. 44 (2016) 355–365.
- [56] C. Rössig, N. Angrisani, P. Helmecke, S. Besdo, J.-M. Seitz, B. Welke, N. Fedchenko, H. Kock, J. Reifenrath, *In vivo* evaluation of a magnesium-based degradable intramedullary nailing system in a sheep model, Acta Biomater. 25 (2015) 369–383.
- [57] T. Wakabayashi, A. Ymamoto, A. Kazaana, Y. Nakano, Y. Nojiri, M. Kashiwazaki, Antibacterial, antifungal and nematicidal activities of rare earth ions, Biol. Trace Elem. Res. 174 (2) (2016) 464–470.
- [58] T.J. Haley, Pharmacology and toxicology of the rare earth elements, J. Pharm. Sci. 54 (5) (1965) 663–670.
- [59] N.S. MacDonald, R.E. Nusbaum, G.V. Alexander, F. Ezmirlian, P. Spain, D.E. Rounds, The skeletal deposition of yttrium, university of california, los angeles campus, school of medicine, Atomic (1951).
- [60] S. Hirano, N. Kodama, K. Shibata, K.T. Suzuki, Metabolism and toxicity of intravenously injected yttrium chloride in rats, Toxicol. Appl. Pharmacol. 121 (2) (1993) 224–232.
- [61] D. Schubert, R. Dargusch, J. Raitano, S.-W. Chan, Cerium and yttrium oxide nanoparticles are neuroprotective, Biochem. Biophys. Res. Commun. 342 (1) (2006) 86–91.
- [62] F. Albaaj, A. Hutchison, Lanthanum carbonate (Fosrenol[®]): a novel agent for the treatment of hyperphosphataemia in renal failure and dialysis patients, Int. J. Clin. Pract. 59 (9) (2005) 1091–1096.
- [63] J. Yang, Q. Liu, L. Zhang, S. Wu, M. Qi, S. Lu, Q. Xi, Y. Cai, Lanthanum chloride impairs memory, decreases pCaMK IV, pMAPK and pCREB expression of hippocampus in rats, Toxicol. Lett. 190 (2) (2009) 208–214.
- [64] A. Rachid, M. Christophe, B.-M. Marc, O. Laure, T. Sylvie, P. Paul, Methemoglobinemia by cerium nitrate poisoning, Burns 32 (8) (2006) 1060–1061.
- [65] K.T. Rim, K.H. Koo, J.S. Park, Toxicological evaluations of rare earths and their health impacts to workers: a literature review, Saf. Health Work 4 (1) (2013) 12–26.
- [66] A. Pałasz, P. Czekaj, Toxicological and cytophysiological aspects of lanthanides action, Acta Biochim. Pol. 47 (4) (2000) 1107–1114.
- [67] J. Zhang, H. Li, W. Wang, H. Huang, J. Pei, H. Qu, G. Yuan, Y. Li, The degradation and transport mechanism of a Mg-Nd-Zn-Zr stent in rabbit common carotid artery: a 20-month study, Acta Biomater. 69 (2018) 372–384.
- [68] C. Yuksel, S. Ankarali, N.A. Yuksel, The use of neodymium magnets in healthcare and their effects on health, Northern Clinics of Istanbul 5 (3) (2018) 268.
- [69] R.J. Palmer, J.L. Butenhoff, J.B. Stevens, Cytotoxicity of the rare earth metals cerium, lanthanum, and neodymium in vitro: comparisons with cadmium in a pulmonary macrophage primary culture system, Environ. Res. 43 (1) (1987) 142–156.
- [70] S. Weilin, S. Xiuying, M. Xiying, Effects of samarium on liver and kidney of rats, J. Rare Earth 24 (1, Supplement 1) (2006) 415–418.
- [71] P.M. Anderson, G.A. Wiseman, A. Dispenzieri, C.A. Arndt, L.C. Hartmann, W.A. Smithson, B.P. Mullan, O.S. Bruland, High-dose samarium-153 ethylene diamine tetramethylene phosphonate: low toxicity of skeletal irradiation in patients with osteosarcoma and bone metastases, J. Clin. Oncol. 20 (1) (2002) 189-196
- [72] F. Li, Y. Wang, Z. Zhang, J. Sun, H. Xiao, Distribution of samarium and ytterbium in rats measured by enriched stable isotope tracer technique and Inaa, J. Radioanal. Nucl. Chem. Art. 251 (3) (2002) 437–441.
- [73] C.R. Patra, S.S. Abdel Moneim, E. Wang, S. Dutta, S. Patra, M. Eshed, P. Mukherjee, A. Gedanken, V.H. Shah, D. Mukhopadhyay, In vivo toxicity studies of europium hydroxide nanorods in mice, Toxicol. Appl. Pharmacol. 240 (1) (2009) 88–98.
- [74] Y. Ogawa, S. Suzuki, K. Naito, M. Saito, E. Kamata, A. Hirose, A. Ono, T. Kaneko, M. Chiba, Y. Inaba, Toxicity study of europium chloride in rats, J. Environ. Pathol Toxicol. Oncol. 14 (1) (1995) 1–9.
- [75] T.J. Haley, N. Komesu, G. Colvin, L. Koste, H.C. Upham, Pharmacology and toxicology of europium chloride, J. Pharm. Sci. 54 (4) (1965) 643–645.
- [76] P. Chellan, P.J. Sadler, The elements of life and medicines, Philos. Trans. A Math. Phys. Eng. Sci. 373 (2037) (2015) 20140182.
- [77] B. Song, Y. Wu, M. Yu, P. Zhao, C. Zhou, G.E. Kiefer, A.D. Sherry, A europium (III)-based paracest agent for sensing singlet oxygen by MRI, Dalton Trans. 42 (22) (2013) 8066–8069.
- [78] E.J. Bernstein, C. Schmidt-Lauber, J. Kay, Nephrogenic systemic fibrosis: a systemic fibrosing disease resulting from gadolinium exposure, Best Pract. Res. Clin. Anaesthesiol. 26 (4) (2012) 489–503.
- [79] A. Shinohara, M. Chiba, M. Kikuchi, Determination of terbium in organs of mice administered terbium chloride: comparative study of fluorometry and atomic absorption spectrometry, J. Anal. Toxicol. 13 (3) (1989) 135–140.

- [80] T.J. Haley, N. Komesu, A.M. Flesher, L. Mavis, J. Cawthorne, H.C. Upham, Pharmacology and toxicology of terbium, thulium, and ytterbium chlorides, Toxicol. Appl. Pharmacol. 5 (4) (1963) 427–436.
- [81] R.P. Baum, A. Singh, M. Benešová, C. Vermeulen, S. Gnesin, U. Köster, K. Johnston, D. Müller, S. Senftleben, H.R. Kulkarni, Clinical evaluation of the radiolanthanide terbium-152: first-in-human pet/ct with 152Tb-DOTATOC, Dalton Trans. 46 (42) (2017) 14638-14646.
- [82] R. Ojemann, G. Brownell, W. Sweet, Possible radiation therapy of cephalic neoplasms by perfusion of short-lived isotopes. II. dysprosium-165: metabolism in mouse and cat, Neurochirurgia (Stuttg.) 4 (1) (1961) 41–57.
- [83] Z. Endre, J. Allis, G. Radda, Toxicity of dysprosium shift reagents in the isolated perfused rat kidney, Magn. Reson. Med. 11 (2) (1989) 267–274.
- [84] A.D. Watson, The use of gadolinium and dysprosium chelate complexes as contrast agents for magnetic resonance imaging, J. Alloys Compd. 207-208 (1994) 14-19
- [85] P.W. Durbin, Distribution of the transuranic elements in mammals, Health Phys. 8 (6) (1962) 665–671.
- [86] T.J. Haley, L. Koste, N. Komesu, M. Efros, H.C. Upham, Pharmacology and toxicology of dysprosium, holmium, and erbium chlorides, Toxicol. Appl. Pharmacol. 8 (1) (1966) 37–43.
- [87] Y. Lotan, M.T. Gettman, K. Ogan, L.A. Baker, J.A. Cadeddu, Clinical use of the holmium: yag laser in laparoscopic partial nephrectomy, J. Endourol. 16 (5) (2002) 289–292.
- [88] J.M.H. Teichman, K.F. Chan, P.P. Cecconi, N.S. Corbin, A.D. Kamerer, R.D. Glickman, A.J. Welch, Erbium: YAG versus holmium: yag lithotripsy, J. Urol. 165 (3) (2001) 876–879.
- [89] A. El-Sherif, T. King, Soft and hard tissue ablation with short-pulse high peak power and continuous thulium-silica fibre lasers, Lasers Med. Sci. 18 (3) (2003) 139–147.

- [90] A.Z. Thomas, L. Smyth, D. Hennessey, F. O'Kelly, D. Moran, T.H. Lynch, Zero ischemia laparoscopic partial thulium laser nephrectomy, J. Endourol. 27 (11) (2013) 1366–1370.
- [91] J. Taylor, J. Kieser, Forensic odontology: Principles and Practice, John Wiley & Sons. 2016.
- [92] T.J. Haley, N. Komesu, M. Efros, L. Koste, H.C. Upham, Pharmacology and toxicology of lutetium chloride, J. Pharm. Sci. 53 (10) (1964) 1186–1188.
- [93] J.L. Sessler, W.C. Dow, D. O'Connor, A. Harriman, G. Hemmi, T.D. Mody, R.A. Miller, F. Qing, S. Springs, K. Woodburn, Biomedical applications of lanthanide (III) texaphyrins lutetium (III) texaphyrins as potential photodynamic therapy photosensitizers, J. Alloys Compd. 249 (1–2) (1997) 146–152.
- [94] Z. Liu, T. Ma, H. Liu, Z. Jin, X. Sun, H. Zhao, J. Shi, B. Jia, F. Li, F. Wang, 177Lu-la-beled antibodies for EGFR-targeted spect/ct imaging and radioimmunotherapy in a preclinical head and neck carcinoma model, Mol. Pharm. 11 (3) (2014) 800–807
- [95] J. Emsley, Nature's Building blocks: an A-Z Guide to the Elements, Oxford University Press, Oxford, UK, 2011.
- [96] Dong Bian, Jiuxu Deng, Nan Li, Xiao Chu, Yang Liu, Wenting Li, Hong Cai, Peng Xiu, Yu Zhang, Zhenpeng Guan, Yufeng Zheng, Yuhui Kou, Baoguo Jiang, Rongshi Chen, In vitro and in vivo studies on biomedical magnesium low-alloying with elements gadolinium and zinc for orthopedic implant applications, ACS Appl. Mater. Interfaces 10 (2018) 4394–4408.
- [97] Yang Liu, Xiao Liu, Nicholas Farrell, Dafu Chen, Yufeng Zheng, Comparative, real-time in situ monitoring of galvanic corrosion in mg-mg₂ca and mg-mgzn₂ couples in hank's solution, Corros Sci (2019) revised.